الاية

﴿ بِسْم اللهِ الرَّحْمَنِ الرَّحِيمِ ﴿ 1 ﴾

سورة الفاتحة (1-7)

Dedications

The words and measures can never express my deepest gratitude to my parents. They have been a force of strength all along, and without them it would have been an uphill task for me to complete this work.

Last but not the least, I am deeply indebted to our brothers, sisters and my friends; their incessant support made me achieve new heights in life and built my character.

ACKNOWLEDGEMENTS

All our thanks to Allah Almighty who gave us the strength, Determination, health and granted us with patience to successfully complete of this research.

I cannot express enough thanks to my supervisor for his continued guidance, support and encouragement: Dr. Fragoon Mohammed ahmed. I offer my sincere appreciation for the learning opportunities provided by you.

my completion of this project could not have been accomplished without the support of my colleges, parents and friends. my deepest gratitude. Your encouragement when the times got rough are much appreciated and duly noted.

Abstract

Recent advancement in genomic technologies has opened a new realm for early detection of diseases that shows potential to overcome the drawbacks of manual detection technologies. Computer based malarial parasite analysis and classification has opened a new area for the early malaria detection that showed potential to overcome the drawbacks of manual strategies. This thesis presents a method for automatic classification of malarial infected cells. Blood cell segmentation and morphological analysis is a challenging due complexity of the blood cells. To improve the performance of malaria parasite segmentation and classification, we have used different set of features which are forward to the ANFIS classifier for malaria classification, the segmentation of clustered partially overlapping objects with a shape initially separated using marker controlled watershed segmentation accompanied with and overlapping cells concave point segmentation and contours are approximated using an ellipse, whereas ANFIS classifier for classification on different set of texture and shape features. This Study shows 96.33% and 96.31% recognition rates for both training and testing using ANFIS classifier.

المستخلص

لقد اظهر التقدم الأخير في التقنيات الجينومية عالم جديد للكشف المبكر عن الأمراض الذي اظهر القدرة على التغلب على عيوب الكشف اليدوي. فقد ادي التحليل الالي وتصنيف طفيل الملاريا الي طرق جديدة للكشف عنه في وقت مبكر للتغلب على عيوب الطرق اليدوية. تقدم هذه الرسالة طريقة للتصنيف التلقائي للخلايا المصابة بالملاريا، تقسيم خلايا الدم والتحليل الشكلي لها والذي يمثل تحديا نتيجة للشكل المعقد لخلايا الدم . ولتحسين عملية التقسيم والتحليل الشكلي للملاريا، تم استخدام مجموعة مختلفة من خلايا الدم ثم اضيفت الي المصنف ANFIS لتصنيف الخلايا. تمت عملية تقسيم الخلايا المتداخلة جزئيا اولا باستخدام خوار زمية ال Marker-controlled watershed يليها خوار مية فصل الاشكال المتداخلة عن طريق النقاط المقعرة يليها خواريزمية تقدير شكل الخلية باسخدام القطع الناقص .واخيرا استخدم المصنف ANFIS عملية التصنيف بناءا علي مميزات شكلية و تركيبية استخلصت من الخلايا. وهذه الدراسة تظهر دقة مقدار ها %6.33% لعمليتي التدريب والاختبار باستخدام ANFIS.

Table of Contents

الاية	I
Dedications	II
ACKNOWLEDGEMENTS	III
Abstract	IV
المستخلص	V
List of Tables	IX
List of Figures.	X
Abbreviations	XII
1 Introduction	1
1.1 Global Struggle with Malaria	1
1.2 Problem Statement	2
1.3 Objectives	3
1.3.1 Main objective	3
1.3.2 Specific objectives	3
1.4 Thesis outline	3
2 Theoretical Fundamentals	4
2.1 The Malaria Parasitic Life Cycle	4
2.2 Components of the Blood	6
2.2.1 Red blood Cells	6
2.2.2 White Blood Cells	7
2.2.3 Platelets	8

2.3 Pro	evention of Malaria	8
2.4 Tr	eatment Methods	9
2.5 Ex	xisting Diagnostic Methods and Instrumentation	10
2.5.1	The Gold Standard Malaria Diagnostic Test: Giemsa-Stained Per	ipheral
Blood Smea	rs and Microscopy Review	11
2.5.2	Fluorescent Diagnostic Methods	12
2.5.3	Rapid Diagnostic Tests	14
2.5.4	Polymerase Chain Reaction	15
2.5.5	Alternative Diagnostic Methods	16
2.6 Ac	daptive neuro-fuzzy inference system (ANFIS)	16
2.6.1	Architecture of ANFIS	18
2.6.2	Training Process	20
3 Literat	ure Review	21
4 Metho	dology	27
4.1 Im	nage Analysis Module	27
4.2 Im	nage Acquisition	27
4.3 Im	nage Preprocessing	28
4.4 Ce	ell Segmentation	30
4.4.1	Otsu's thresholding	30
4.4.2	Marker controlled Watershed segmentation	31
4.4.3	Segmentation using concave points	33
4.5 Fe	ature Extraction	39
4.5.1	Geometrical features	40
4.5.2	Texture Features	40

	4.6	Classification of infected cells	42
5	Res	sults and discussions	44
	5.1	Results	44
	5.2	Discussions	48
6	Co	nclusion & recommendations	49
	6.1	Conclusion	49
	6.2	Recommendations	49
References		50	
A	ppen	dix A	54
A	ppen	dix B	63

List of Tables

Table No	Title	Page No
Table 1	Summary table of literature methods for Malaria Detection	26
Table 2	Comparison between manual and automated method	47
Table 3	Detection error analysis	47

List of Figures

Figure No	Title	Page No
Figure 1	Female Anopheles mosquito taking a blood meal.	1
Figure 2	Malaria parasite life cycle.	4
Figure 3	Microscopic image of intraerythrocytic P. falciparum merozoites rupturing	
	an RBC membrane to infect additional RBCs and perpetuate the infection	5
	cascade.	
Figure 4	Giemsa-stained Plasmodium falciparum showing hemozoin (green arrow).	5
Figure 5	Scanning electron micrograph of a red blood cell, magnification 11397X.	7
Figure 6	The five types of WBCs. In a normal blood sample, the neutrophil is the	
	most common (40-75%), followed by the lymphocyte (20-45%), monocyte	8
	(3-11%), eosinophil (0-7%), and basophil (0-1%).	
Figure 7	Platelets observed with Wright stain, manifesting as small dark-purple	8
	fragments. A neutrophil is shown at the center of the image.	o
Figure 8	Plasmodium falciparum Giemsa-stained thin film peripheral blood smear.	12
Figure 9	Interfering substances in peripheral blood smears. A. Platelet superimposed	
	on a red blood cell. B. Platelet clump, which can potentially be	12
	misinterpreted as schizonts. C. Schuffners dots in a P. ovale trophozoite. D.	12
	Eosinophil, exhibiting red stip.	
Figure 10	QBC Malaria test showing two trophozoites of P. falciparum (arrows).	13
	Parasitic DNA appears green and the cytoplasm appears yellow-orange.	13
Figure 11	AMRAD (Sydney, Australia) rapid diagnostic test showing a positive result	15
	for P. falciparum (Left) and negative result (Right).	13
Figure 12	Six types of fuzzy membership functions: triangular (A), z-shape (B),	17
	trapezoidal (C), s-shape (D), sigmoid (E) and Gaussian (F).	17
Figure 13	Structure of the proposed ANFIS model.	18
Figure 14	System Architecture.	27
Figure 15	Sample image obtained by leica DFC 295 camera with resolution of	28
	300x300.	20
Figure 16	Image preprocessing Algorithm Flow Diagram.	29

Figure 17	Otsu's method: (a) the input image form morphological reconstruction, (b)	31
	after Appling Otsu's Threshold	31
Figure 18	Marker controlled watershed algorithm.	32
Figure 19	marker controlled watershed segmentation, (a) Otsu image with some	20
	overlapping cells, (b) the result image after separating overlapping cells	32
Figure 20	Concave Point Segmentation Algorithm.	34
Figure 21	Contour segmentation: (a) Edge map; (b) Corner detection; c) Concavity	
	test to extract concave corners (green circle) and removed convex corners	25
	(pink square); (d) Contour segmentation by concave points the colors are	35
	used only for illustrative.	
Figure 22	Segment grouping: (a) Original binary image; (b) Contour segmentation;	
	(c) Segment grouping (the thin gray lines are added to illustrate the	38
	grouping of non-adjacent segments).	
Figure 23	Contour estimation: (a) Original image; (b) Contour evidence extraction;	39
	(c) Contour estimation.	35
Figure 24	one of the test images segmented using concave point and ellipse fitting.	39
Figure 25	Feature Extraction and Classification workflow	43
Figure 26	ANFIS classifier Performance	44
Figure 27	Automatic malaria classification function and its input and output (Green	
	normal, red infected malaria cells).	45
Figure 28	graphical user interface program	46

Abbreviations

ACT Artemisinin Combination Therapies

ADD average distance deviation

AMCC Automatic Malaria Cell Classification

ANFIS Adaptive neuro-fuzzy inference system

ANN Artificial Neural Network

AWGN Additive white Gaussian noise

BCP Benzothiocarboxypurine

CAD computerized aided automated diagnosis

CDC Centers for Disease Control

CSS curvature scale space

CT Computer Tomography

DA De-noising auto-encoder

DAPI 4',6-diamidino-2-phenylindole

DLFANN Direct linked artificial feed-through ANN

DNA deoxyribonucleic acid

FIS fuzzy inference system

FLANN functional link ANN

FN False negative FP False positive

GLCM Gray-Level Co-Occurrence Matrix

GUI graphical user interface

HNN Hopfield neural network

HSV Hue, saturation and value color space

LED Light emitting diode

MF Membership function

MFLANN Modified functional linked ANN

MLP Multilayer perception

NCNN noisy chaotic neural network

NPV Negative prediction value

PCR Polymerase Chain Reaction

PLT Platelets

PPV Positive prediction value

PSO particle swarm optimization

RBC Red blood cells

RDT Rapid diagnostic tests

SCG scaled conjugate gradient

SVM Support vector machine

THG Third Harmonic Generation

TN True negative

TP True positive

WBC White blood cells

Introduction

1.1 Global Struggle with Malaria

Malaria is a common but serious protozoan disease caused by peripheral blood, spleen or liver parasites of the genus Plasmodium. The World Health Organization estimates 300-500 million malaria cases and more than 1 million deaths per year [1]. It is caused by any of the four-different species of Plasmodium parasite, vivax, ovale, malariae and falciparum. Disease is transmitted via the bite of an infected female of the Anopheles mosquito.

Overtreatment of negative patients accelerates the evolution of antimalarial drug resistance, complicates the diagnosis of other acute febrile illnesses, and wastes resources in low-wealth regions that have limited supplies of antimalarial treatment options [2]. A prompt and accurate diagnosis is, therefore, imperative to the control and management of malaria. Delays in diagnosis and treatment are leading causes of malaria-related deaths in several endemic countries, and in non-endemic countries, technicians frequently falsely diagnose a patient due to lack of experience in examining peripheral blood smears for identification of parasitemia [3]. Furthermore, clinicians often doubt microscopy results and continue to treat non-infected patients based on clinical suspicion of the presenting symptoms [2, 4].



Figure 1 Female Anopheles mosquito taking a blood meal.

Detection methods for Malaria can for Malaria be classified into two Categories, based on their cost and performance. These are the high cost methods and low cost methods. Polymerase Chain Reaction (PCR) based techniques that detect specific nucleic acid sequences and Third Harmonic Generation (THG) imaging of emission from the Hemozoin using infrared ultrafast pulsed laser excitation, belong to the class of high cost methods. Studies have shown that these techniques can yield high sensitivity and specificity to malaria diagnosis. However, they are rarely used in developing countries where the disease is endemic because of the high cost, specialized infrastructure needs and handling difficulties. RDTs are relatively fast in malaria diagnosis and can be administered by unskilled personnel. However, their results can be unreliable. Besides, commercially available RDT kits are specific to single species of plasmodium parasites and in cases where mixed infection is suspected, all the four kits should be used to detect deferent Malaria Species. This makes the technique relatively expensive [5]. The most widely used technique for determining the development stage of the malaria disease is visual microscopical evaluation of Giemsa stained blood smears [6]. The obvious limitation of this technique is time consuming. Besides, the results obtained are difficult to reproduce. An automated diagnosis system can be designed by understanding the diagnostic expertise and representing it by specifically tailored image processing, analysis and pattern recognition algorithms. A complete system must be equipped with: image acquisition, preprocessing, segmentation (object localization), and classification tasks. In order to perform diagnosis on peripheral blood samples, the system must be capable of differentiating between malarial parasites, artifacts, and healthy blood components.

1.2 Problem Statement

Conventional microscopy is the gold standard method of malaria diagnosis using giemsa stained blood smears. however, this is a routine and time consuming procedure and requires a trained Technician. Plus, sophisticated techniques for malaria detection are expensive and unaffordable in places where malaria is a serious problem. Parallel to this, less sophisticated techniques are affordable but their results always are not reliable. Besides a recent study on

the field shows the agreement rates among the clinical experts for the diagnosis are surprisingly low.

1.3 Objectives

This Study Has main and Specific objectives as follows.

1.3.1 Main objective

The long-term goal of the research is to develop an accurate automatic malaria detection and classification system which can reduce the overall testing time.

1.3.2 Specific objectives

This research has specific objectives as follows:

- 1. Incorporate multiple segmentation methods for better detection of infected RBCs.
- 2. Classify each RBC contained within the image as infected or not.
- 3. Design a Graphical user interface for ease of use.

1.4 Thesis outline

The thesis accumulates six chapters, the first chapter is the introduction to inform other researchers about thesis problems and objectives, the second chapter is theatrical fundamentals which give readers the required knowledge and tools as walkthrough to the thesis, the third chapter discuss the literature of previous studies and their problem's encountered and how they solve it, the whole thesis was based on their studies, the use of image processing techniques to segment malaria cells and Machine learning capabilities identify malaria parasite, the fourth chapter is the methodology, it's a specific layout of this thesis and how every contribute to final, the fifth chapter is results and discussions which summarizes thesis methodology in statistical results and why and how those results are acquired.

The final chapter is conclusion and recommendations which outline the final outcome and the resultant of the thesis, which objectives are accomplished and how thesis method could be enhanced and developed further more.

Theoretical Fundamentals

2.1 The Malaria Parasitic Life Cycle

The life cycle of the malaria parasite (Figure 2) requires both a vertebrate host and a mosquito for survival. Malaria is spread to humans by an infected female pregnant Anopheles mosquito (Figure 1), which releases sporozoites into the vertebrate host during a blood meal. Sporozoites are highly motile reproductive organisms that travel through the circulatory system and invade the hepatocytes of the liver. An asexual replication process known as schizogony occurs, resulting in the production of tens of thousands (per hepatocyte) of haploid forms, known as merozoites, until the hepatocyte membrane finally ruptures [7].

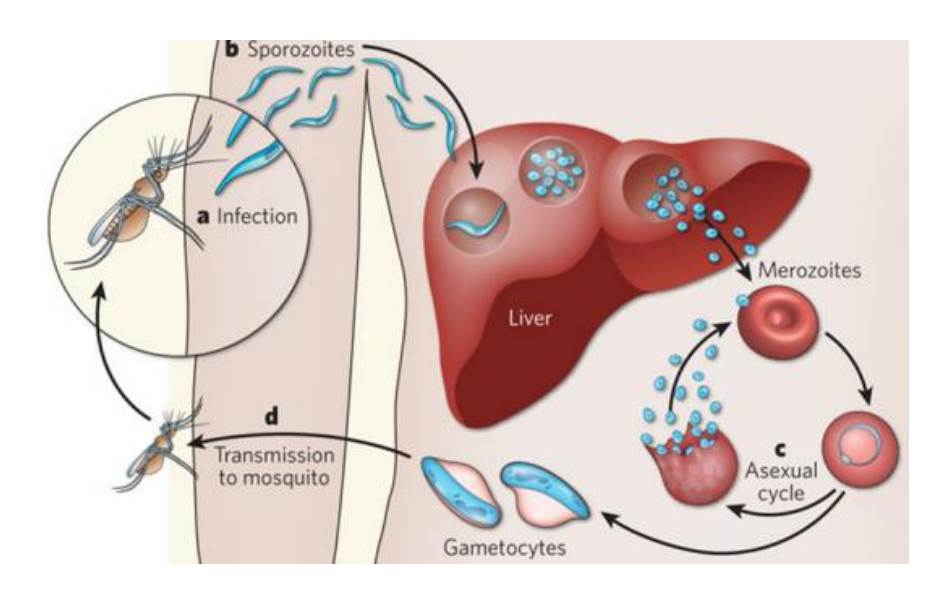


Figure 2 Malaria parasite life cycle.

Merozoites are then released into the blood stream to invade erythrocytes (Figure 3), also known as red blood cells (RBCs), and develop into three morphologically and metabolically distinct stages named rings, trophozoites and schizonts. Merozoites invade RBCs to escape phagocytosis by leukocytes, commonly known as white blood cells (WBCs), and to consume hemoglobin as a protein source for continued replication and survival. Rings are the first intraerythrocytic stage, evolving over the course of several hours into the larger trophozoite form, which upon initiation of asexual reproduction, begins the schizont stage.

Schizonts produce between eight and twenty-four daughter merozoites and ultimately rupture the erythrocytic membrane. Each merozoite is then capable of initiating a new cycle of intraerythrocytic asexual replication in a new RBC, Schizonts are rarely present in peripheral blood of P. falciparum infections, except in severe cases [8]. The repeated cycles of development and multiplication within human erythrocytes is responsible for the pathological symptoms associated with human malaria.



Figure 3 Microscopic image of intraerythrocytic P. falciparum merozoites rupturing an RBC membrane to infect additional RBCs and perpetuate the infection cascade.

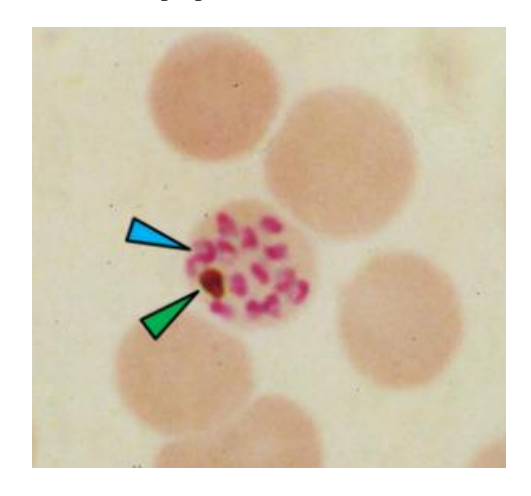


Figure 4 Giemsa-stained Plasmodium falciparum showing hemozoin (green arrow).

During the erythrocytic stage, the malaria parasite consumes hemoglobin and detoxifies heme by forming an insoluble crystalline brown pigment known as hemozoin. Hemozoin is produced in all erythrocytic stages but is only readily detectable in late trophozoites and schizonts.

A critical step in parasite development, which accounts for the large geographic distribution of malaria worldwide and the rapid spread of drug-resistant strains, is the ability of a subpopulation of the parasites within human red blood cells to differentiate into precursor male and female sexual forms called gametocytes. These forms are transmitted to a female Anopheles mosquito during a blood meal. Mating between male and female gametocytes takes place within the mosquito stomach and is followed by meisois and a series of asexual divisions to produce oocysts, each harboring thousands of new sporozoites. In a process known as gliding motility, the sporozoites migrate to the salivary glands of the mosquito to infect another vertebrate host during another blood meal [9]. This perpetuates the malaria life cycle.

2.2 Components of the Blood

Considering malaria's inhabitance within the systemic circulation, the components of blood should be discussed in further detail to provide the reader with sufficient background knowledge.

Blood is an essential fluid for oxygen and nutrient transportation to and metabolic waste uptake from the cells of the body. It is comprised of three cell types: RBCs, WBCs, and platelets, all of which are suspended in plasma, a clear to yellow liquid comprised mostly of water, dissolved proteins, and cell nutrients.

2.2.1 Red blood Cells

RBCs provide the critical function of delivering oxygen to tissues and circulate throughout the human body for approximately 120 days before being filtered by the kidneys when their supporting proteins are no longer viable [10]. RBCs primarily consist of hemoglobin, a metalloprotein responsible for oxygen uptake and distribution throughout the body. Hemoglobin has four identical sub-units, each with a heme component, globin chain,

and an iron atom bound to the heme [10]. Oxygen has a high affinity to loosely and reversibly bind with iron, thereby enabling RBCs to efficiently transport oxygen molecules.

The cellular structure of the RBC is beneficial to its primary functions (Figure 5). The plasma membrane provides sufficient structure while maintaining compliance, allowing cells to circulate through narrow capillary beds. The biconcave shape optimizes the surface area to improve oxygen transfer across the plasma membrane. RBCs also expel their nucleus during erythropoiesis to allow for maximal hemoglobin content, but immature cells may consist of reticular material for a short period of time while in circulation.

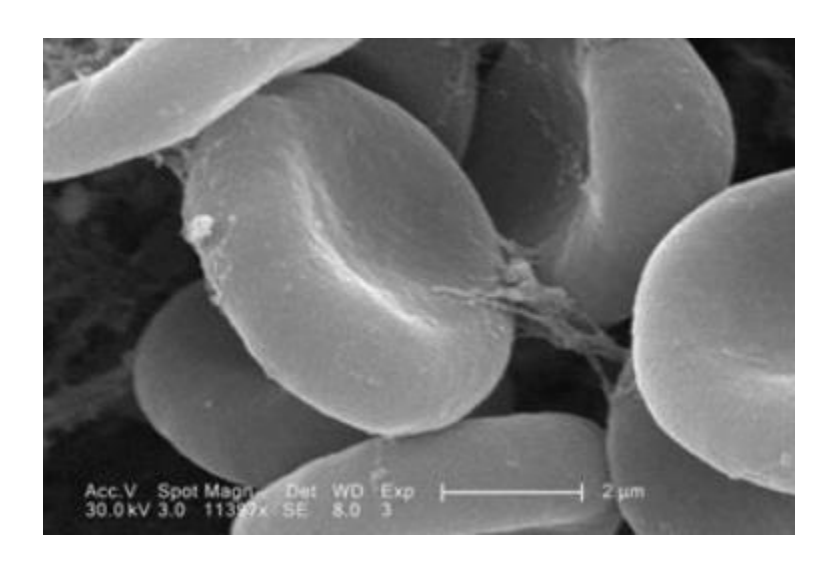


Figure 5 Scanning electron micrograph of a red blood cell, magnification 11397X.

2.2.2 White Blood Cells

WBCs, shown pictorially in (Figure 6), are responsible for the immune response to infection [10]; they are subdivided into five subpopulations: neutrophils, lymphocytes, monocytes, eosinophils, and basophils. WBCs are capable of attacking extracellular parasites; however, once a parasite has invaded an RBC, it becomes invisible to most immune responses.

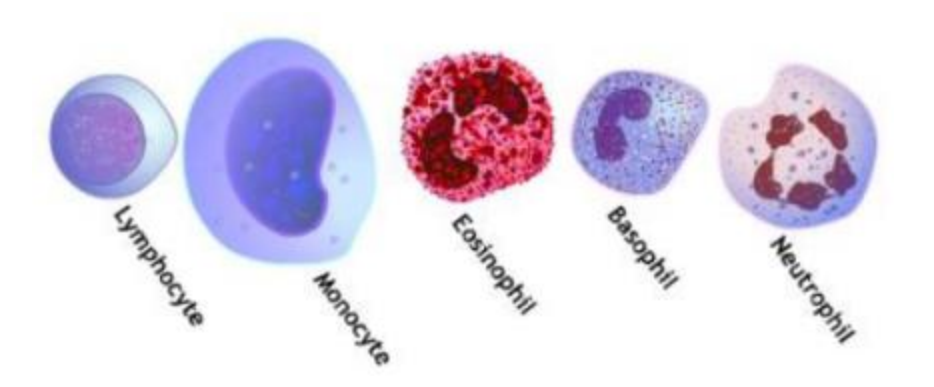


Figure 6 The five types of WBCs. In a normal blood sample, the neutrophil is the most common (40-75%), followed by the lymphocyte (20-45%), monocyte (3-11%), eosinophil (0-7%), and basophil (0-1%).

2.2.3 Platelets

Platelets are cell fragments from megakaryocytes that contribute to hemostasis and blood clotting activity [10]. They are shown in (Figure 7) in a Wright stained microscopic image, a common laboratory stain for peripheral blood smear analysis.

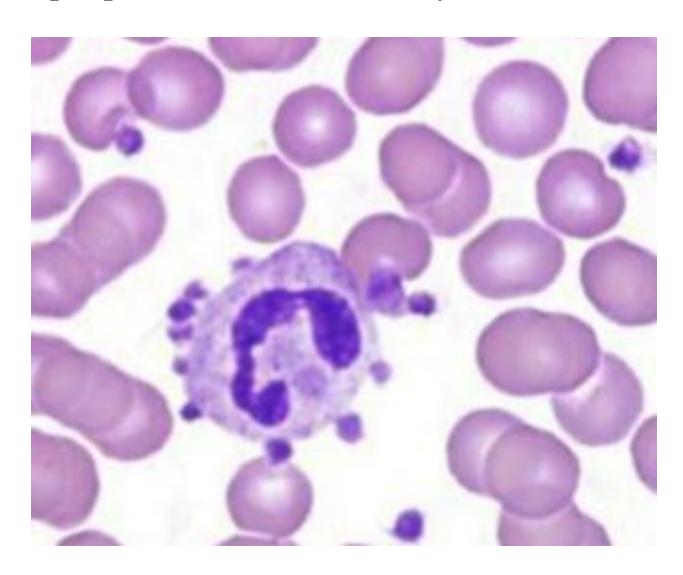


Figure 7 Platelets observed with Wright stain, manifesting as small dark-purple fragments. A neutrophil is shown at the center of the image.

2.3 Prevention of Malaria

The use of insecticides, insecticide-treated bed nets, and drug therapies has and will continue to decrease the prevalence and mortality rate associated with malaria [11,12]. However, many populations throughout the world remain at a significant risk of infection because the mosquito resistance to insecticides and artemisinin may contribute to a surge of as

many as 26 million new annual cases [13, 14]. There is no malaria vaccine currently approved for human use but advancements in medical research and technology may offer capabilities to finally eradicate this disease in the future [11]. Accurate diagnostics also contribute to the prevention of malaria because, the sooner a patient can be diagnosed with malaria, the sooner that patient can be treated with antimalarial to eradicate the parasite, preventing subsequent disease transmission.

2.4 Treatment Methods

Malaria treatment depends on several factors, including disease severity, the Plasmodium species, the clinical status of the patient, pregnancy, and the geographic region in which the infection was acquired [15]. Intravenous and oral drugs, such as chloroquine, quinine, quinidine, doxycycline, and Artemisinin Combination Therapies (ACT), are generally successful at eradicating uncomplicated cases but certain species of malaria exhibit drug resistance that render some treatments ineffective. ACTs, for example, have demonstrated a 95% cure rate in nonresistant uncomplicated falciparum malaria cases [16]; however, recent resistance development to artemisinin is concerning and may have severe repercussions. Artemisinin was previously capable of clearing malaria parasites from a patient within 24 hours, but now requires three to four days for a complete treatment [17]. In the near future, some patients may not respond to artemisinin at all. Complicating matters further is the prevalence of counterfeit anti-malaria drugs, which contributes to inadequate treatment for the patient and increases the risk of drug resistance development [18].

Treatment based solely on symptoms and without proper diagnosis contributes to resource waste, drug resistance development, and the unnecessary exposure of patients without clinical malaria to antimicrobial agents [19, 2]. Further complicating matters is the fact that many people carry and transmit the disease but are asymptomatic of malaria and are not treated [12]. Furthermore, due to the increased cost of newer and more effective drugs, such as artemisinin, diagnostic methods have become vitally important to efficient distribution in resource poor regions [2]. The interested reader should refer to the Guidelines for Treatment of Malaria in the United States published by the Centers for Disease Control and Prevention

for additional information on prevention and treatment methods [20]. An accurate laboratory diagnosis and knowledge of disease severity, stage progression, and Plasmodium species is imperative in formulating a treatment protocol [21]. A screening method such as the one proposed in this thesis would permit early diagnosis and treatment of malaria, potentially before the onset of symptoms and disease transmission to another individual. This will help contribute to vector control and by extension, prevent malaria infection.

2.5 Existing Diagnostic Methods and Instrumentation

There are numerous methods available today for the diagnosis of malaria. Each method has its own unique set of advantages and disadvantages, but, to date, an optimal method does not exist. Socioeconomic factors, durability and stability, and distribution limitations are just some of the challenges facing malaria diagnosis. Two of the most important parameters for a malaria diagnostic test are sensitivity and specificity, both of which are statistical measures of the performance of a binary classification test (i.e., whether or not the patient is infected with malaria). Sensitivity is the proportion of correctly identified positives and is given by:

$$Sensitivity = \frac{TP}{TP + FN} \tag{1}$$

while specificity is the proportion of correctly identified negatives and is given by:

$$Specificity = \frac{TN}{TN + FP} \tag{2}$$

Where TP is the occurrence of true positives, TN is the occurrence of true negatives, FP is the occurrence of false positives, and FN is the occurrence of false negatives. Two measures closely related to sensitivity and specificity are positive predictive value (PPV) and negative predictive value (NPV). The PPV is the proportion of positive test results that are correct and is given by:

$$PPV = \frac{TP}{TP + FP} \tag{3}$$

Conversely, NPV is the proportion of negative test results that are correct and is given by:

$$NPV = \frac{TN}{TN + FN} \tag{4}$$

The PPV and NPV of a particular test can provide a clinician with a level of confidence in regards to the accuracy of a given result. Other features such as parasite morphology assessment, species differentiation, and parasitemia estimation are available in certain methods depending on the diagnostic technology of the test or system. Current diagnostic methods were analyzed in a comprehensive literature review to determine the shortcomings of existent technology and help formulate new ideas to address these issues. A summary of significant findings is described in the following sections.

2.5.1 The Gold Standard Malaria Diagnostic Test: Giemsa-Stained Peripheral Blood Smears and Microscopy Review

The current gold standard for detection of Plasmodium employs Giemsa staining of thin and thick blood smears with conventional light microscopy [22] (Figure 8). Giemsa is specific to the phosphate groups of DNA and attaches to regions of high adenine-thymine bonding, yielding a high-contrast parasitic visualization. Microscopy review of Giemsa stains is the most commonly-performed laboratory diagnostic test due to its simplicity, relatively low cost, ability to differentiate parasitemia, and manual determination of parasitemia magnitude [3]. Microscopic review of peripheral blood smears suffers from inherent flaws that severely inhibit efficacy in diagnosing malaria. Most importantly, the sensitivity of microscopy is typically no greater than 75% to 90%, and in some settings, can be as low as 50% [19, 2]. Low parasitemia levels further complicate Giemsa staining [23], as the average microscopist can only detect 50 to 100 parasites per microliter [24]. Reviewing peripheral blood smears is time-consuming (30 to 60 minutes) and requires a trained observer to interpret parasitemia, thereby limiting its capability for high-throughput screening. Inadequate staining and poor microscopy methods can degrade the visualization of the parasite making it more difficult for species differentiation. Artifacts in blood can often be mistaken for malaria parasites even if proper staining techniques are performed (Figure 9) [25]. The most frequent mistake is the misidentification of platelets that are superimposed on red blood cells as malaria parasites. Their appearance is similar but

platelets can be differentiated based on the absence of chromatin dots and refrainment patterns when focusing. Eosinophils can often be confused with P. ovale and P. vivax trophozoites because eosinophilic stippling is similar in appearance to Schuffners dots. Dust particles, stain deposits, obscuring debris, and blood cell ghosts are other common artifacts that may confuse the microscopist. Despite these insufficiencies, it is still the most common method for detecting Plasmodium parasites, with over 165 million peripheral smears performed in 2010 [19].

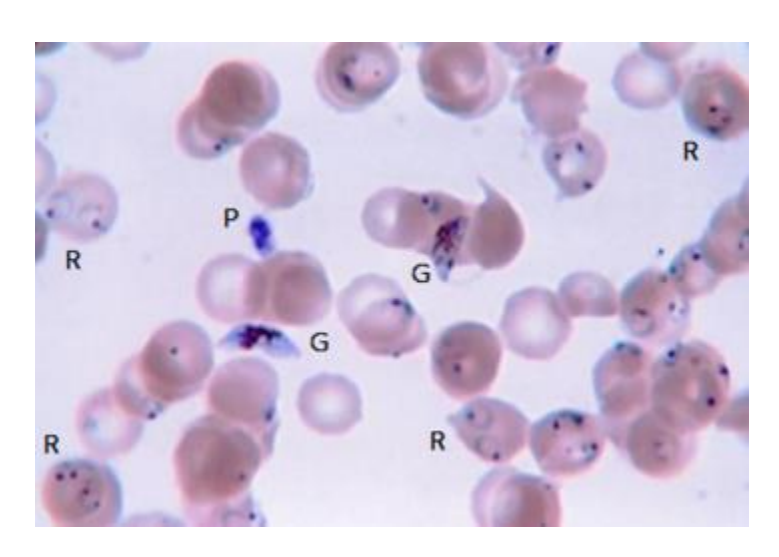


Figure 8 Plasmodium falciparum Giemsa-stained thin film peripheral blood smear.

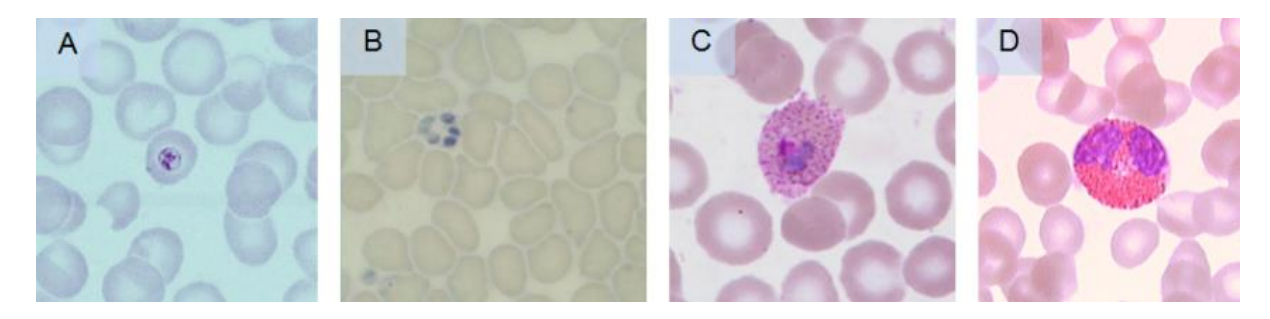


Figure 9 Interfering substances in peripheral blood smears. A. Platelet superimposed on a red blood cell. B. Platelet clump, which can potentially be misinterpreted as schizonts. C. Schuffners dots in a P. ovale trophozoite. D. Eosinophil, exhibiting red stip.

2.5.2 Fluorescent Diagnostic Methods

Fluorescent stains such as acridine orange, DAPI, and benzothiocarboxypurine (BCP) have demonstrated efficacy in malaria diagnosis when conventional light microscopes are fixed with an interference filter. This method offers advantages particularly evident in conditions of low parasitemia. The rate of staining and observation is increased and the training level

required to achieve consistent and reliable results is decreased. Excessive cost and availability of materials are limiting to these methods and a trained observer is still required for interpretation of results [26, 27, 6]. The nucleic-acid selective stain, acridine orange, has been successfully applied to the Quantitative Buffy Coat [28]. system for rapid diagnosis of malaria and other parasitic infections with an eightfold increase in lower detection limits compared to Giemsa-stained thick smears [23]. In this method, blood specimen is stained with acridine orange in a micro hematocrit tube. After centrifugation, a clear plastic float, with a specific gravity equal to that of the buffy coat (WBC layer), settles to the buffy coat layer and expands this region up to ten-fold. RBCs infected with malarial parasites are less dense, and therefore occupy the space near the buffy coat - RBC interface. Centrifugal stratification concentrates the parasites into a discrete region (1 to 2 mm) and retains the parasites close to the tube wall so they may be visualized using a fluorescence microscope with an LED illumination attachment known as the Para Lens (QBC Diagnostics) (Figure 10) [29, 30]. Since the parasites are concentrated from a relatively large volume of blood (50 to 110 mL, compared to 5 mL for peripheral smears), the sensitivity is increased and the examination time required to confirm or disprove infections is decreased. in [30] demonstrated that, after centrifugation is complete (5 minutes at 12,000 g), only 7 to 10 minutes are required for review to confirm that the sample is negative, and [29] demonstrated that less than one minute is required to confirm a positive infection.

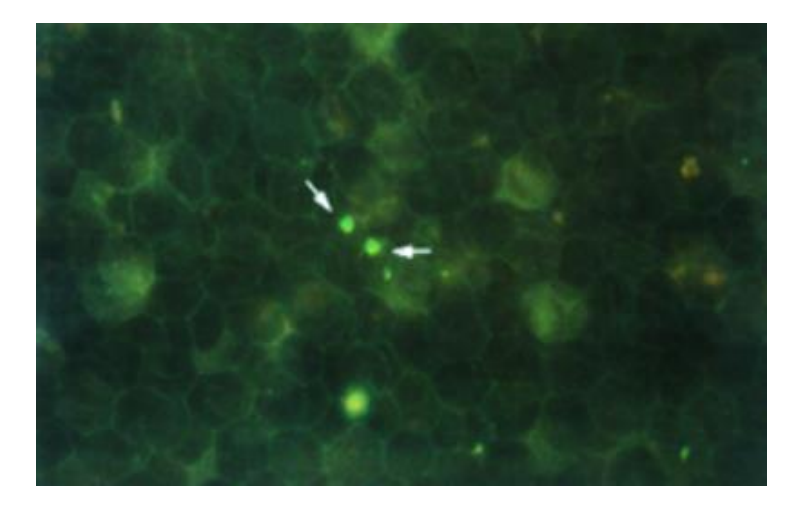


Figure 10 QBC Malaria test showing two trophozoites of P. falciparum (arrows). Parasitic DNA appears green and the cytoplasm appears yellow-orange.

2.5.3 Rapid Diagnostic Tests

Rapid diagnostic tests (RDTs) offer a simple, prompt, accurate, and cost-effective diagnostic test for identifying malaria parasitemia by the detection of three distinct Plasmodium antigens. Plasmodium histidine-rich protein II (pHRP-2) is specific to P. falciparum and P. Vivax. Plasmodium lactate dehydrogenase (pLDH) is likewise specific to P. falciparum and P. vivax, but its isomers can also be used to detect all Plasmodium species (i.e., pan specific). Finally, Plasmodium aldolase is also pan specific. The combination of these antigens can be used to detect the presence of P. falciparum, P. vivax, or any combination thereof [19]. To perform a test, blood specimen is placed on a nitrocellulose strip with antibodies dispersed in well-defined lines (Figure 11). The lysed specimen migrates down the strip and if it contains Plasmodium parasites, the complex of the antibodies and parasite antigens generates visible indicators to demonstrate a positive test result. A labeled goat antibody capture provides a control method to indicate that the test is functioning properly [31]. Malaria diagnosis by RDTs has been reported as excellent [3], but there are several deficiencies with this method. First, non-falciparum infections may be misdiagnosed as negative for malaria if the RDT only contains pHRP-2. Multiple immunochromatographic tests must be combined when using RDTs to ensure that all species of malaria may be detected. There are also variants of P. falciparum in South America that do not produce HRP-2 and therefore cannot be detected using an RDT. Cross-reactions have been reported for patients with Schistosoma mekongi infection, rheumatoid factor or other auto-antibodies. Additionally, RDTs cannot be used to measure parasitemia magnitude, therefore the severity of the disease is not known to the clinician unless a peripheral smear is reviewed. Finally, RDTs are inefficient at diagnosing low parasitemia, which may lead to a false diagnosis and further symptom development by the patient. These limitations generally require the clinician to use RDTs in conjunction with other diagnostic methods for confirmation of reported results, characterization of infection, and to monitor the progress of patients undergoing anti-malarial treatment [3].

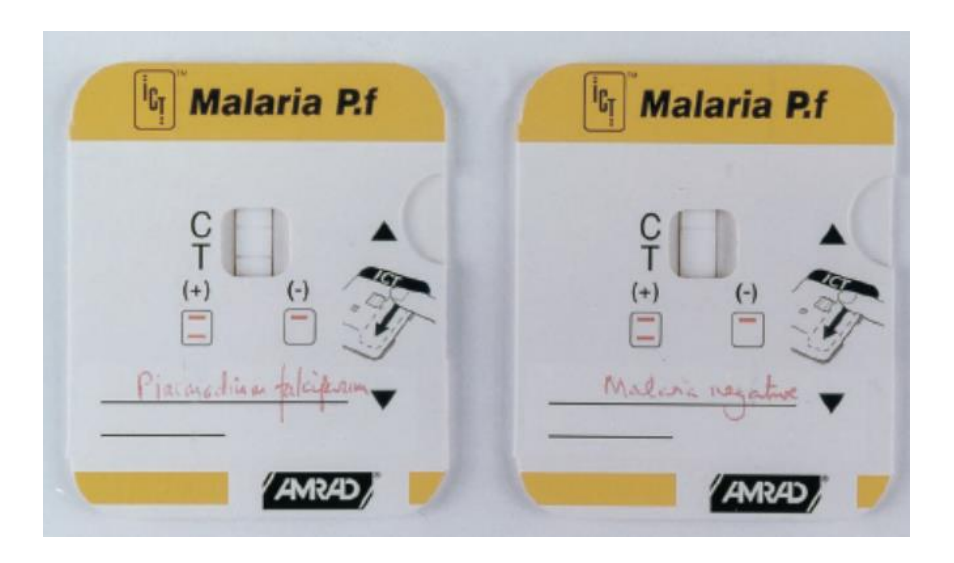


Figure 11 AMRAD (Sydney, Australia) rapid diagnostic test showing a positive result for P. falciparum (Left) and negative result (Right). [31]

2.5.4 Polymerase Chain Reaction

Polymerase Chain Reaction (PCR) is a relatively new malaria diagnostic method that has been documented to be one of the most sensitive and specific tests especially in case of low parasitemia [3]. It is common practice to utilize PCR as a confirmatory method in advanced laboratories due to its superior performance to Giemsa staining [3]. Briefly, PCR is a process wherein the DNA of the parasite is amplified to several orders of magnitude greater. A process known as thermal cycling repeatedly heats and cools the sample to enable DNA melting and the subsequent enzymatic replication of the malaria DNA. PCR has demonstrated an ability to detect as little as five parasites per mL, or 0.001 % parasitemia, assuming a 5 x 106. It is important to note that the availability of PCR is limited in low wealth endemic regions due to its complex methodology, high cost, time-intensive procedure (i.e., >24 hours) and need for trained technicians [3, 31]. Quality control and regular maintenance is also a requirement of PCR, further limiting its potential for malaria diagnosis in rural areas. It is, therefore, mostly reserved for research and, occasionally, diagnostic purposes in large clinics and hospitals.

2.5.5 Alternative Diagnostic Methods

Other diagnostic methods such as serological, Loop-Mediated Isothermal PCR (LAMP), microarrays, flow cytometry, automated blood cell counters, and mass spectrophotometry are less commonly used. They each offer some distinct advantages but have significant limitations that diminish their effectiveness as malarial diagnostic methods.

2.6 Adaptive neuro-fuzzy inference system (ANFIS)

The fuzzy set theory developed by (Zadeh, 1965) provides as a mathematical framework to deal with vagueness associated with the description of a variable. The commonly used fuzzy inference system (FIS) is the actual process of mapping from a given input to output using fuzzy logic. Fuzzy logic is particularly useful in the development of expert systems. Expert systems are built by capturing the knowledge of humans: however, such knowledge is known to be qualitative and inexact. Experts may be only partially knowledgeable about the problem domain, or data may not be fully available, but decisions are still expected. In these situations, educated guesses need to be made to provide a solution to the problems. This is where fuzzy logic can be employed as a tool to deal with imprecision and qualitative aspects that are associated with problem solving [32]. A fuzzy set is a set without clear or sharp boundaries or without binary membership characteristics. Unlike a conventional set where object either belongs or do not belong to the set, partial membership in a fuzzy set is possible. In other words, there is a softness associated with the membership of elements in a fuzzy set [32]. A fuzzy set may be represented by a membership function. This function gives the grade (degree) of membership within the set. The membership function maps the elements of the universe on to numerical values in the interval [0, 1]. The membership functions most commonly used in control theory are triangular, trapezoidal, Gaussian, sigmoidal membership functions show in Figure 12 [33, 34, 35].

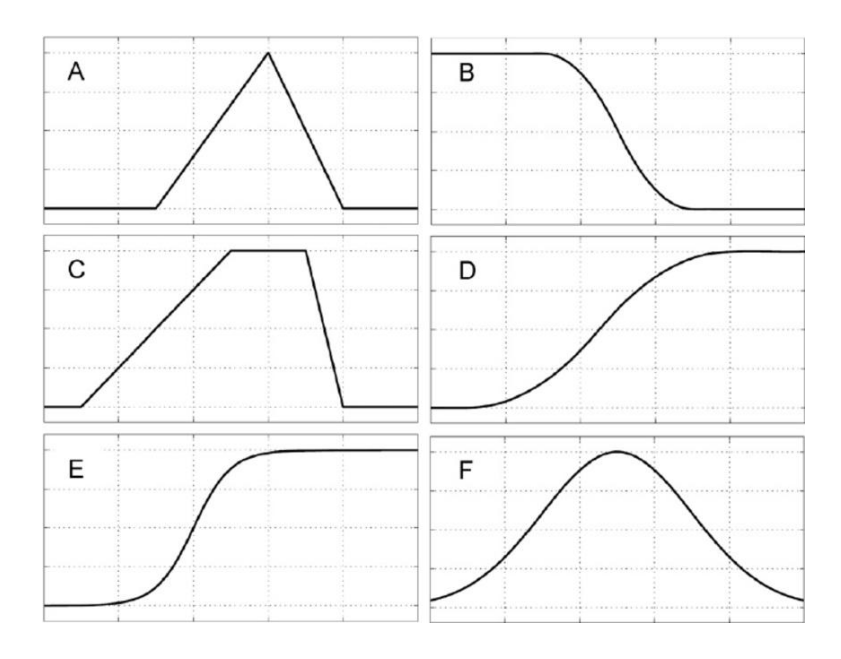


Figure 12 Six types of fuzzy membership functions: triangular (A), z-shape (B), trapezoidal (C), s-shape (D), sigmoid (E) and Gaussian (F).

As mentioned previously, the fuzzy inference system is the process of formulating the mapping from a given input to an output using fuzzy logic. The dynamic behavior of an FIS is characterized by a set of linguistic description rules based on expert knowledge. The fuzzy system and neural networks are complementary technologies. The most important reason for combining fuzzy systems with neural networks is to use the learning capability of neural network. While the learning capability is an advantage from the view point of a fuzzy system, from the viewpoint of a neural network there are additional advantages to a combined system. Because a neuro-fuzzy system is based on linguistic rules, we can easily integrate prior knowledge in to the system, and this can substantially shorten the learning process. One of the popular integrated systems is an ANFIS, which is an integration of a fuzzy inference system with a back-propagation algorithm [32, 36]. There are two types of fuzzy inference systems that can be implemented: Mamdani-type and Sugeno-type [37, 38]. Because the Sugeno system is more compact and computationally more efficient than a Mamdani system, it lends itself to the use of adaptive techniques for constructing the fuzzy models. These adaptive techniques can be used to customize the membership functions so that the fuzzy system best models the data. The fuzzy inference system based on neuro-adaptive learning techniques is termed adaptive neuro-fuzzy inference system [39]. In order for an FIS to be mature and well

established so that it can work appropriately in prediction mode, its initial structure and parameters (linear and non-linear) need to be tuned or adapted through a learning process using a sufficient input-output pattern of data. One of the most commonly used learning systems for adapting the linear and nonlinear parameters of an FIS, particularly the first order Sugeno fuzzy model, is the ANFIS. ANFIS is a class of adaptive networks that are functionally equivalent to fuzzy inference systems [32].

2.6.1 Architecture of ANFIS

(Figure 12) shows the architecture of a typical ANFIS with two inputs X1 and X2, two rules and one output f, for the first order Sugeno fuzzy model, where each input is assumed to have two associated membership functions (MFs). For a first-order Sugeno fuzzy model a typical rule set with two fuzzy if—then rules can be expressed as [32]:

Rule (1): If X_1 is A_1 and X_2 is B_1 , then $f_1 = m_1 X_1 + n_1 X_2 + q_1$,

Rule (2): If X_1 is A_2 and X_2 is B_2 , then $f_2 = m_2 X_1 + n_2 X_2 + q_2$.

where: m_1 , n_1 , q_1 and m_2 , n_2 , q_2 are the parameters of the output function.

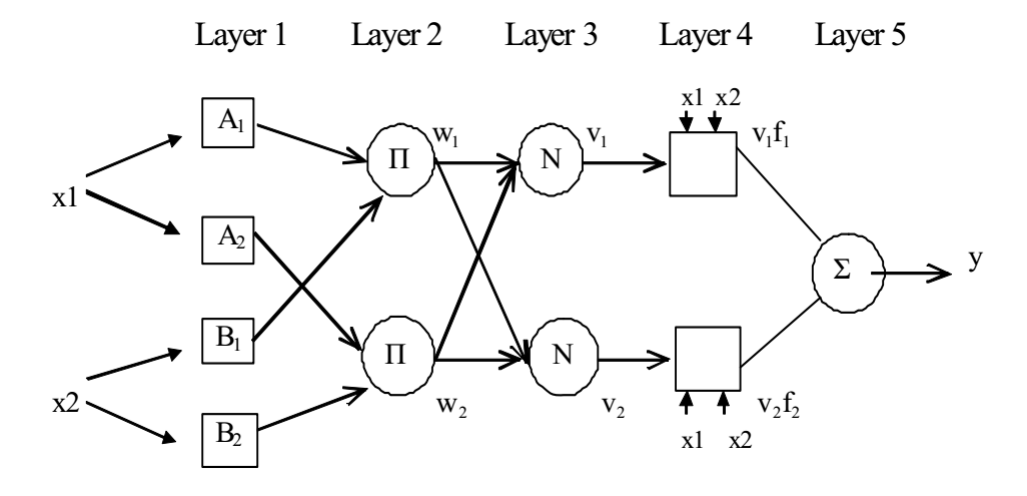


Figure 13 Structure of the ANFIS model.

It contains five layers where the node functions in the same layer are of the same function family. Inputs, outputs and implemented mathematical models of the nodes of each layer are explained below.

Layer 1: This layer performs fuzzification of the inputs, The node function of every node i in this layer take the form:

$$Q_i^1 = \mu A_i(X) \tag{5}$$

where X is the input to node i, μA_i is the membership function (which can be triangular, trapezoidal, gaussian functions or other shapes) of the linguistic label A_i associated with this node and O_i is the degree of match to which the input X satisfies the quantifier Ai. In the current study, the Gaussian shaped MFs defined below are utilized.

$$\mu A_i(X) = exp\left\{-\frac{1}{2}\frac{(X-C_i)^2}{\sigma_i^2}\right\} \tag{6}$$

where $\{C_i, \sigma_i\}$ are the parameters of the MFs governing the Gaussian functions. The parameters in this layer are usually referred to as premise parameters.

Layer 2: Every node in this layer multiplies the incoming signals from layer 1 and sends the product out as follows,

$$w_i = \mu A_i(X_1) \times \mu B_i(X_2), i = 1,2 \tag{7}$$

where the output of this layer (w_i) represents the firing strength of a rule.

Layer 3: Each neuron in this layer calculates the normalized degree of truth of the fuzzy rule, every node i in this layer is a node labeled N, determine the ratio of the i-th rule's firing strength to the sum of all rules' firing strengths as:

$$v_i = \frac{w_i}{w_1 + w_2}, i = 1,2 \tag{8}$$

where the output of this layer represents the normalized firing strengths.

Layer 4: Every node i in this layer is an adaptive node with a node function of the form:

$$Q_i^4 = w_i^- f_i = w_i^- (m_i X_1 + n_i X_2 + q_i), i = 1,2$$
 (9)

where w_i^- is the output to layer 3, and $\{m_i, n_i, q_i\}$ is the parameter set of this node. Parameters in this layer are referred to as consequent parameters.

Layer 5: There is only a single node in this layer that computes the overall output as the weighted average of all incoming signals from layer 4 as:

$$Q_i^5 = \sum_{i} w_i^- f_i = \frac{\sum_{i} w_i f_i}{\sum_{i} w_i}, i = 1,2$$
 (10)

2.6.2 Training Process

As mentioned earlier, both the premise (non-linear) and consequent (linear) parameters of the ANFIS should be tuned, utilizing the so-called learning process, to optimally represent the factual mathematical relationship between the input space and output space. Normally, as a first step, an approximate fuzzy model is initiated by the system and then improved through an iterative adaptive learning process. Basically, ANFIS takes the initial fuzzy model and tunes it by means of a hybrid technique combining gradient descent backpropagation and mean least-squares optimization algorithms. At each epoch, an error measure, usually defined as the sum of the squared difference between actual and desired output, is reduced. Training stops when either the predefined epoch number or error rate is obtained. There are two passes in the hybrid learning procedure for ANFIS. In the forward pass of the hybrid learning algorithm, functional signals go forward till layer 4 and the consequent parameters are identified by the least squares estimate. In the backward pass, the error rates propagate backward and the premise parameters are updated by the gradient descent. When the values of the premise parameters are learned, the overall output (f) can be expressed as a linear combination of the consequent parameters [33]:

$$f = \frac{w_1}{w_1 + w_2} f_1 + \frac{w_2}{w_1 + w_2} f_2 = w_1^- f_1 + w_2^- f_2$$

$$= (w_1^- X_1) m_1 + (w_1^- X_2) n_1 + (w_1^-) q_1 + (w_2^- X_2) m_2$$

$$+ (w_2^- X_2) n_2 + (w_2^-) q_2$$
(11)

which is linear in the consequent parameters m_1 , n_1 , q_1 , m_2 , n_2 and q_2 .

Literature Review

A literature survey summarizes all the relevant literature researched during the course of this project. It presents certain approaches used by many researchers for classification. It also compares the performance of all classifier with other common classifier with same parameters. Finally, the best parameters and classifier combination is discussed. Lucy Gitonga, et al [40] introduces a technique for identifying the parasites life stages and species using microscopic images of thin blood smears stained with Giemsa was developed. The technique entailed designing and training Artificial Neural Network (ANN) classifiers to perform the classification of infected erythrocytes into their respective stages and species. The system recorded 99.9% in recognizing stages and 96.2% in recognizing plasmodium species. Daniel Maitethia Memeu, et al [41] proposes an accurate, speedy and affordable system of malaria detection using stained thin blood smear images was developed. The method uses Artificial Neural Net- work (ANN) to test for the presence of plasmodium parasites in thin blood smear images. Images of infected and non-infected erythrocytes were acquired, preprocessed, relevant features extracted from them and eventually diagnosis was made based on the features extracted from the images. Classification ac- curacy of 95.0% in detection of infected erythrocyte was achieved with respect to results obtained by expert microscopist. Magudeeswaran Veluchamy, et al [42] describes the method of evaluating the clinical status is counting of cell types based on features that it contains. There is a need for a rapid, reproducible method, superior to human inspection and for the classification of cells. For solving these problems, quantitative digital-image analysis is applied and a novel method for classifications of affected blood cells from normal in an image of a microscopic section is presented. These blood cell images are acquired from different patient with sickle cell anemia, sickle cell disease and normal volunteers. Approach: The segmentation of blood cells is made by morphological operations such as thresholding, erosion and dilation to preserve shape and size characteristics. In addition, we use back propagation neural network to classify the blood cells more efficiently.

Dipti D. Patankar, et al [43] presents automatic methods for detection and classification of malarial parasites in thin blood smear. For this Artificial Neural Network (ANN) and

Bayesian Network (BN) are used as promising techniques. Morphological features such as shape, size are considered to identify infected erythrocytes and possible type of plasmodium. ParasChawla, et al [44]. In order to use medical images for the diagnosing process, it must be noiseless. However, most of the images are affected by noises and artifacts. In order to achieve this de-noising of CT images, an effective CT image de-noising technique is proposed. The proposed technique removes the Additive white Gaussian Noise from the CT images and improves the quality of images. The proposed work is comprised of three phases; they are preprocessing, training and testing. In the preprocessing phase, the CT image which is affected by the AWGN noise is transformed using multi wavelet transformation. In the training phase the obtained multi-wavelet coefficients are given as input to the Adaptive Neuro-Fuzzy Inference System (ANFIS). Sudhansu Kumar Mishra, et al [45] presents an alternate ANN structure called functional link ANN (FLANN) for imaged noising. In contrast to a feed forward ANN structure i.e.a multilayer perceptron (MLP), the FLANN is basically a single layer structure in which non-linearity is introduced by enhancing the input pattern with nonlinear function expansion. In this work three different expansions are applied. Yazeed A. Al-Sbou, et al [46] describes the image de-noising is a challenging task in the digital image processing research and application. This makes it imperative to find a robust method to comply that task. In this paper, a detailed performance evaluation of using the neural networks as a noise reduction tool is presented. Suchitra Sarangi, et al [47] discusses image restoration is an important part of image processing in which it presents a functional link artificial neural network based technique for image restoration which has the capacity of reducing the Gaussian noise present in an image. Then a comparison has been carried out between the proposed filter & the other existing filter. Junyuan Xie, et al, [48] propose a novel approach to low-level vision problems that combines sparse coding and deep networks pre-trained with de-noising autoencoder (DA). We propose an alternative training scheme that successfully adapts DA, originally designed for unsupervised feature learning, to the tasks of image de-noising and blinding painting. Snigdha Mohanty, et al [49] describes design the four artificial neural networks(ANNs) for de-noising of digital image corrupted with AWGN or salt and pepper noise is presented, and then using a Multilayer perceptron(MLP) using the popular back

propagation algorithm, Direct Linear Artificial Feed-through Neural Network (DLFANN), Functional Link Artificial Neural Network (FLANN) and Modified-Functional Link Artificial Neural Network (MFLANN)have been implemented in this regard and extensive computer simulation have been carried out for performance comparison among these algorithms. Leipo Yan, et al [50] proposes new approach to address image de noising based on a new neural network, called noisy chaotic neural network (NCNN). The original Bayesian framework of image de-noising is reformulated into a constrained optimization problem using continuous relaxation labelling. The NCNN, which combines the simulated annealing technique with the Hopfield neural network (HNN), is employed to solve the optimization problem. Sheenum Marwaha, et al, [51] provides a brief review of computerized aided automated diagnosis techniques which use Digital Image Processing, their benefits and the types of diseases diagnosed by these systems. However, CAD system is having many problems, so new methods need to be introduced by combining the benefits of other classification techniques with CAD. Ms. Deepali Ghate, et al, [52] discusses computerized diagnosis, which will help in immediate detection of the disease to some extent, so that the proper treatment can be provided to the malaria patient. Also the image processing algorithm is used which will reliably detect the presence of malaria parasite from Plasmodium falciparum species in thin smears of Giemsa stained peripheral blood sample. S. S. Savkare, et al, [53] presents an automatic technique is proposed for Malaria parasites detection from blood images by extracting red blood cells (RBCs) from blood image and classifying as normal or parasite infected. Manual counting of parasite is tedious and time consuming and need experts. Proposed automatic approach is used Otsu thresholding on gray image and green channel of the blood image for cell segmentation, watershed transform is used for separation of touching cells, color and statistical features are extracted from segmented cells and SVM binary classifier is used for classification of normal and parasite infected cells. Pallavi T. Suradkar, et al, [54] reviews image analysis studies aiming at automated diagnosis or screening of malaria infection in microscope images of thin blood film smears. Malaria is a mosquito-borne infectious disease of humans and other animals caused by parasites (a type of microorganism) of the genus Plasmodium. Infection is initiated by a bite from an infected female mosquito, which introduces the parasites via its saliva into

the circulatory system, and ultimately to the liver where they mature and reproduce. Deepa.A.Kurer, et al, [55] presents the image processing algorithm to automate the diagnosis of malaria in blood images is developed in this project. The image classification system is designed to positively identify malaria parasites present in thin blood smears, and differentiate the species of malaria.

[56] Illustrate a technique for identifying the malaria for blood cell images, which involves counting of Blood cell using an adaptive OTSU thresholding technique. Which use to segment the image and separate the RBC and WBC. The paper also considers the area of cells to declare severity and uses SVM as Classifier for declaring the result of whether the patient is affected by Malaria or Not. An approach is proposed to detect red blood cells with consecutive classification into parasite infected and normal cells for estimation of parasitemia. The extraction of red blood cells achieves a reliable performance and the actual classification of infected cells. Sensitivity of system is 93.12%, and Specificity is 93.17%. Shape based and statistical features are generated for classification. The features are selected for recognition of two classes only. This approach leads to the high specialization of each classifier and results in an overall increase in accuracy. Makkapati and Rao [58] explored the segmentation for HSV color space. A scheme presented in [57] is based on HSV color space that segments Red Blood Cells and parasites by detecting dominant hue range and by calculating optimal saturation thresholds. Methods those are less computation-intensive than existing approaches are presented to remove artifacts. The scheme is evaluated using images taken from Leishmanstained blood smears. Sensitivity of the scheme was found to be 83%. The method operates in HSV space and is dynamic in the sense that relevant thresholds are determined from the statistics of the given image rather than keeping them fixed for all images. Schemes determine optimal saturation thresholds to segment RBCs and chromatin dots that are robust with respect to the color variability encountered. The work in [57] illustrates the use of color image processing techniques. Raviraja et al. [58] introduces a blood image processing for detecting and classifying malarial parasites in images of Giemsa stained blood slides, in order to evaluate the parasitemia of the blood. To detect the red blood cells that are infected by malarial parasites,

statistical based approach is used. To separate automatically the parasites (trophozoites, schizonts and gametocytes) from the rest of an infected blood image, color, shape and size information are used and later the image is compared with infected images after transformation of image by scaling, shaping to reconstruct the image. The images returned are statistically analyzed and compare to generate a mathematical base. Also, the evaluation of the size and shape of the nuclei of the parasite is also considered. Ruberto et al. [59] introduces morphological approach to cell image segmentation more accurate than the normal watershed based algorithm. The used non-flat disk-shape structuring element enhanced the roundness and compactness to improving the accuracy of normal watershed based algorithm whereas flat disk-shape structuring element to separate overlapping cells. These methods make use of knowledge of the RBC structure that is not used in existing watershed based algorithm. In [59] a scheme based on RGB color space that segments Red Blood Cells and parasites by detecting dominant hue range and by calculating optimal saturation thresholds is presented. Methods that are less computation intensive than existing approaches are proposed to remove artifacts. The scheme is evaluated using images taken from Leishman-stained blood smears. Sensitivity of the scheme is found to be 83%. Automated image analysis-based software. Malaria Count. for parasitemia determination, i.e. for quantitative evaluation of the level of parasites in the blood, has been described in [59]. The presented system is based on the detection of edges representing cell and parasite boundaries. The described technique includes a preprocessing step, edge detection step, edge linking, clump splitting, and parasite detection.

Table 1 Summary table of literature methods for Malaria Detection

Reference	Target	Preprocessing	Segmentation	Features	Classificatio	Accuracy
Article	Data		Method		n	
publisher					Method	
Lucy Gitonga	Parasite	Digital zooming,	Using hue and	Statistical	Artificial	99.9% stages
	Life stages	contrast	saturation optimum	features	neural	96.2% parasite
		enhancement and	thresholds		network	detection
		mean filter				
Maitethia	Presence of	Digital zooming,	thresholding	Direct pixel	Artificial	95% accuracy
Memeu	plasmodium	and mean filter		values, shape	neural	
				based and	network	
				texture based		
Magudeeswa	Counting blood	-	Morphological	Statistical	back	
ran	cells based on		operation and edge	based, shape	propagation	80% accuracy
Veluchamy	its features		detection	based and	ANN	
				texture based		
Dipti D.	Detection and	Median filter	Color based	Morphologic	ANN and	
Patankar	classification of		segmentation	al features	Bayesian	
	malaria parasite			(size, shape)	network	
S. S.	Automatic	Mean filter and	Otsu's threshold	Color	SVM	83.75%
Savakare	malaria	Green plane	and watershed	statistical		accuracy
	detection	selection		features		
Shiff	Identifying	Mean filter and	Otsu's thresholding	HSV	SVM	93.12
	malaria in blood	HSV color space		statistical		sensitivity and
	images	conversion		features		93.17
						Specificity
Amit Kumar	Detection of red	Mean filter and	Optimum	-	-	83% accuracy
	blood cells and	HSV color space	saturation			
	infected	conversion	thresholds			
	parasites					
Ravirja	Detecting and	Color normalization	Morphological	Statistical	k-nearest	74% sensitivity,
	classifying		thresholding	based and	neighbor	98% specificity
	malarial			shape based	classifier	
	parasites			features		
Ruberto	Morphological	-	Watershed and	-	-	-
	cell		non-flat disk shape			
	segmentation					

Methodology

4.1 Image Analysis Module

Due to complexity of the blood sample images, malarial parasite segmentation and morphological analysis is a challenging problem. Machine vision based malarial diagnostic methods has been widely studied in order to provide early and accurate diagnose of malaria parasite. An ideal diagnostic method would be accurate, non-invasive, and inexpensive. The key tasks for malarial parasite classification involve segmenting the malaria parasite infected cells from the complicated background. The system block diagram is shown in Figure 13.

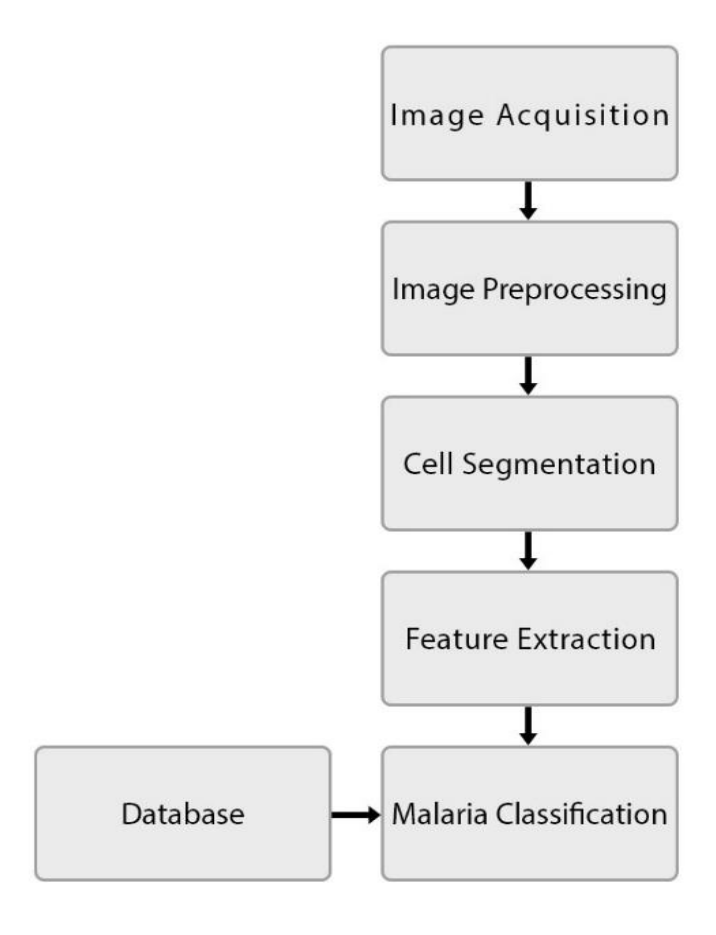


Figure 14 Image Analysis Module.

4.2 Image Acquisition

A number of thick blood films was prepared using Giemsa staining technique. it is a rapid staining method for screening of parasites. The sensitivity of a thick blood film is 5-10

parasites/µl. Thin blood films stained by Giemsa's is useful for specification of parasites and for the stippling of infected red cells and have a sensitivity of 200 parasites/µl. The optimal pH of the stain is 7.2. The requirements need for film preparation are Giemsa stain powder, 100% Methanol, Bibulous paper, Microscope with x100 oil immersion lens (Olympus CX21). The preparation of stain procedure was followed as recommended by Khartoum laboratory Administration in the following order: first fixing the slider in 100% methanol for ~30" and rinse off in tap water, then Make up a fresh solution of 10% Giemsa stain in distilled water, Stain for ~30" and Rinse off slide in tap water and dry thoroughly using bibulous paper to dab. now for screening part View slide under oil immersion with a 100x objective. Images were acquired using a camera attached to the microscope which is a Leica DFC 295 camera and acquire the 1000x magnified image form the oil immersion lens maintaining a constant image size of 300x300 pixels.

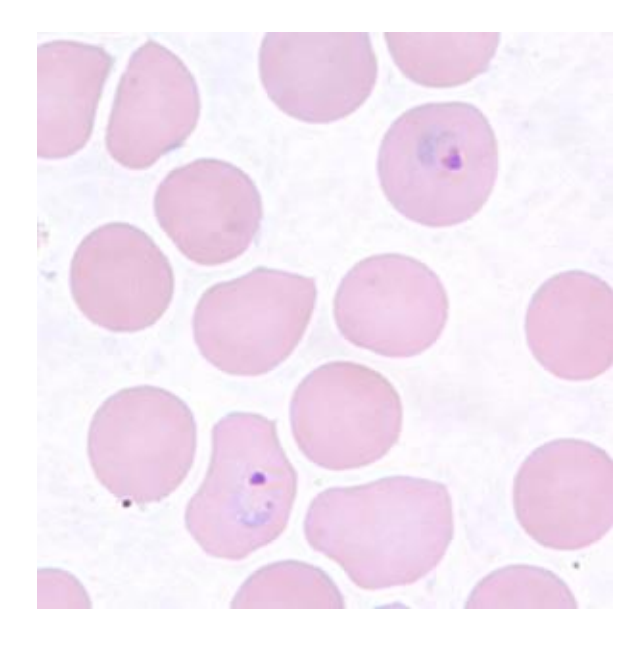


Figure 15 Sample image obtained by leica DFC 295 camera with resolution of 300x300.

4.3 Image Preprocessing

Blood smear images might be affected by illumination and color distribution of blood images due to the varieties of digital camera and staining variability. Most of the microscopes provide uniform or relatively uniform illumination images. The aim of preprocessing step is to obtain images with low noise, high contrast than original images for the further processing.

This particular problem poses difficulties for classification of blood cells since it is hard to deal with proper segmentations of objects with quite similar colors. This process contains two operations image enhancement and noise reduction.

Morphological techniques called "opening-by-reconstruction" and "closing-by-reconstruction" was applied to clean up image noise and eliminate non-uniform background illumination, by using disk shaped element with a radius of 2 pixels to apply a morphological erosion to the image, the result is Ie. Then the image is reconstructed by Ie with help of matlab function "imreconstruct", the result image is Ir.

Next Appling a morphological dilation to Ir by the same disk shaped structure element Ird, then Appling a morphological reconstruction to both Ird and Ir complements, the result is Irr. finally obtaining the complement of Irr.

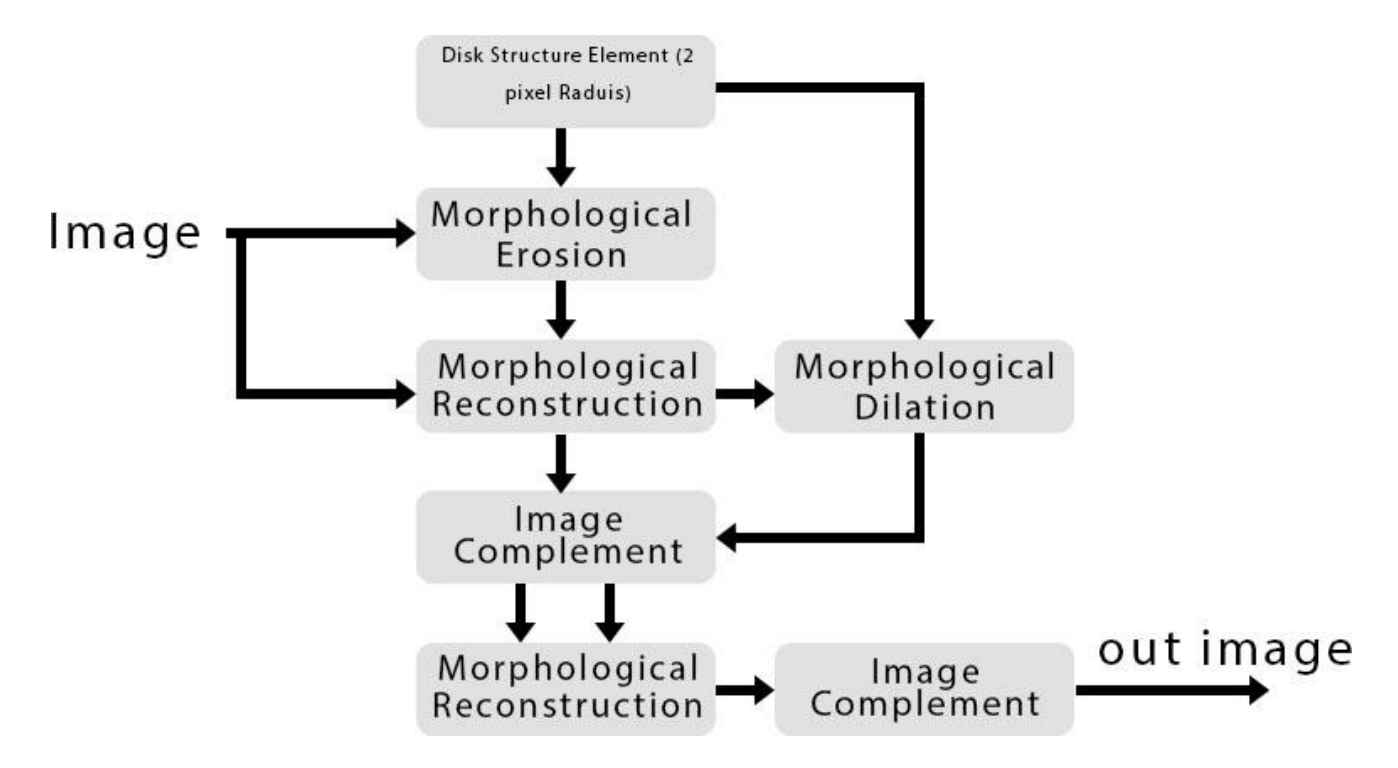


Figure 16 Image preprocessing Algorithm Flow Diagram.

4.4 Cell Segmentation

In the analysis of automatic classification of malarial parasite procedures, the most important and difficult part is segmentation of malaria parasite infected blood cells from the background and other cells because the blood cells are often overlaid with each other and is the basis of quantitative analysis of its deformability and hence its filterability [61]. Cell shapes, light variation and noise are the other factors that make segmentation a difficult task. Accurate segmentation allows fruitful result in sub-sequent levels. Malarial parasite lies in erythrocytes thus we need to segment the erythrocyte form the blood images.

4.4.1 Otsu's thresholding

This method was used for background and foreground segmentation; Otsu's method reduces image's gray level to a binary image. The algorithm assumes that the image contains two classes of pixels following bi-modal histogram (foreground pixels and background pixels), it then calculates the optimum threshold separating the two classes so that their combined spread intra-class variance is minimal, or equivalently (because the sum of pairwise squared distances is constant and shows that minimizing the intra-class variance is the same as maximizing inter-class variance: [62]

$$\sigma_b^2 = \omega_0(t)\omega_1(t)[\mu_0(t) - \mu_1(t)]^2 \tag{12}$$

Where $\omega_{0,1}$ are the probabilities of the two classes separated by a threshold t and $\mu_{0,1}$ are the mean of two classes. The green image plane was selected because it contains high contrast RBCs version of the image. Then Appling Otsu's method as shown in figure 16:

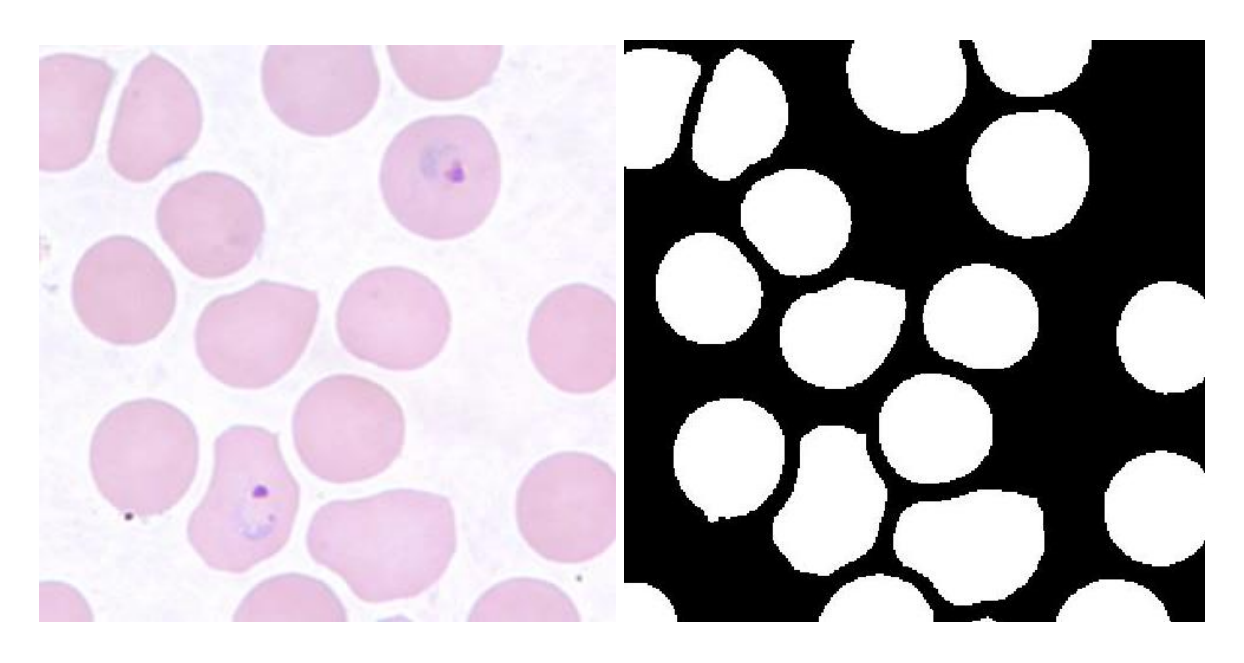


Figure 17 Otsu's method: (a) the input image form morphological reconstruction, (b) after Appling Otsu's Threshold

4.4.2 Marker controlled Watershed segmentation

Some images in this study have multiple overlapping cells, and those appear as one cell, and that poses a problem later in classification section.

Two combination methods were used to separate cells, the first one watershed segmentation, this algorithm considers the input image as a topographic surface (where higher pixel values mean higher altitude) A watershed is a basin-like landform defined by highpoints and ridgelines that descend into lower elevations and stream valleys [63].

It's not suitable to use the algorithm directly because it results in over segmentation, is a well-known phenomenon in watershed segmentation. Over segmentation occurs because every regional minimum, even if tiny and insignificant, forms its own catchment region. One solution is to modify the image to remove minima that are too shallow. So, an enhanced watershed technique also known as marker controller watershed was used, it relies on a marker image to simulates its flooding algorithm. The local minima of the image's pixel distance were used as a marker.

Chessboard distance transform was applied to Otsu's image to simulate every object in the image as valleys, this transform also known as Chebyshev distance is a metric defined on a vector space where the distance between two vectors is the greatest of their differences along any coordinate dimension. In two dimensions, i.e. plane geometry, if the points p and q have Cartesian coordinates (x_1, y_1) and (x_2, y_2) , their Chebyshev distance is:

$$D_{chess} = \max(|x_2 - x_1|, |y_2 - y_1|) \tag{13}$$

The marker controller watershed algorithm is shown in figure 17:

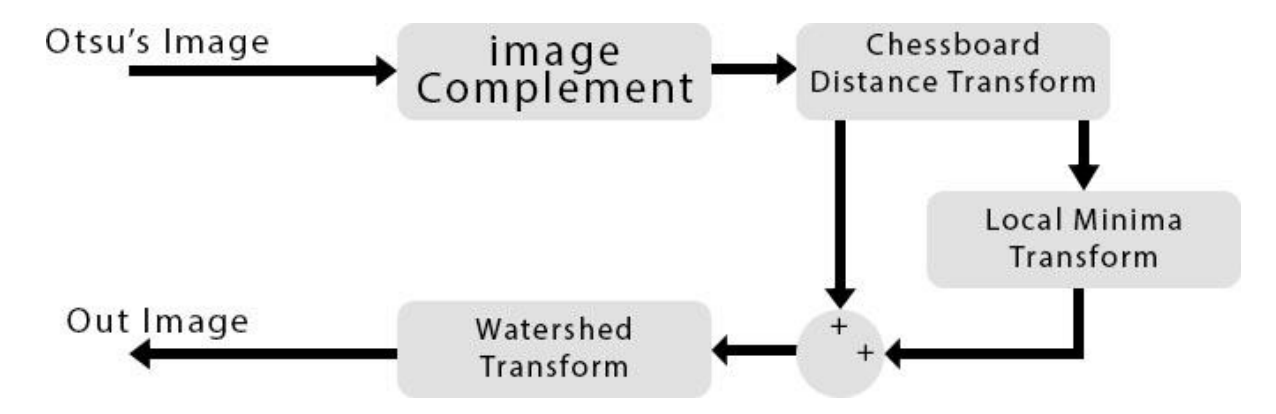


Figure 18 Marker controlled watershed algorithm.

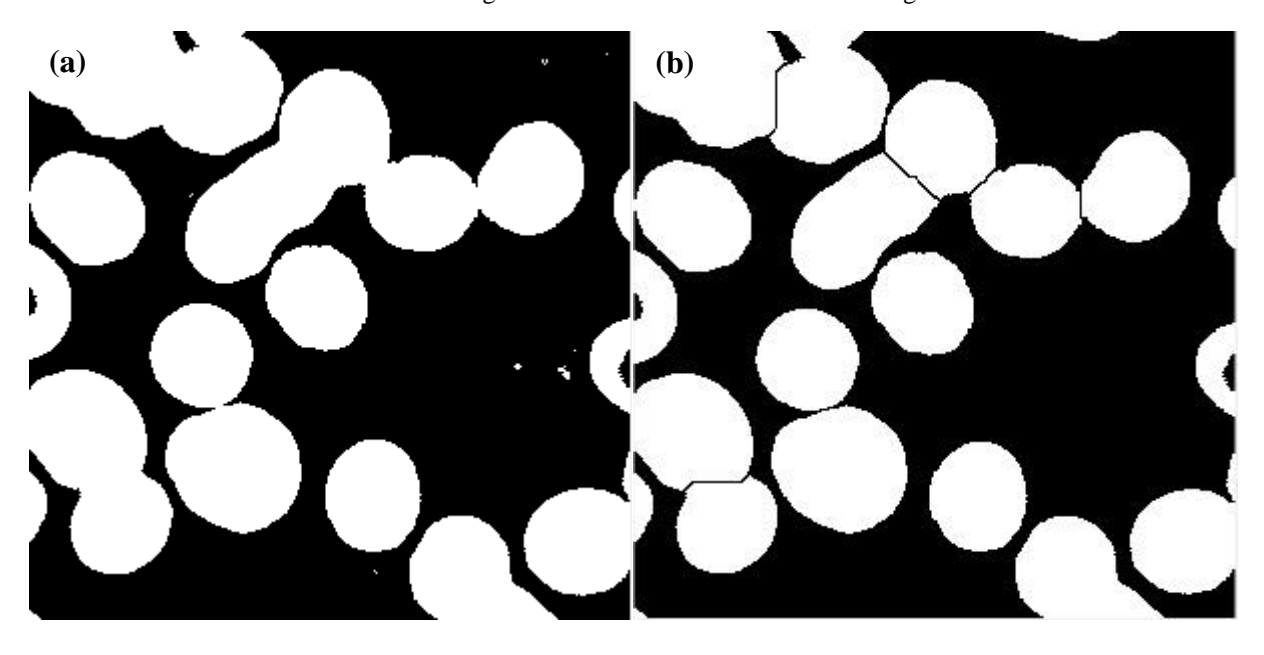


Figure 19 marker controlled watershed segmentation, (a) Otsu image with some overlapping cells, (b) the result image after separating overlapping cells

4.4.3 Segmentation using concave points

Segmentation of overlapping objects aims to address the issue of representation of multiple objects with partial views. Overlapping or occluded objects occur in various applications, such as morphology analysis of molecular or cellular objects in biomedical and industrial imagery where quantitative analysis of individual objects by their size and shape is desired [64–66]. In many such applications, the objects can often be assumed to have approximately elliptical shape.

The watershed transform is one of the commonly used approaches in overlapping cell segmentation. However, methods based on the watershed transform suffer from a poor or inadequate initialization and may experience difficulties with segmentation of highly overlapped objects in which a strong gradient is not present.

In [67] a novel and efficient method is proposed for the segmentation of partially overlapping RBCs with a convex shape. The RBCs are assumed to be clearly distinguishable from the background of the image and their contours form approximately elliptical shapes. The proposed method relies on two sequential steps of contour evidence extraction and contour estimation. The contour evidence extraction step is further divided into two sub-steps: contour segmentation and segment grouping. In the contour segmentation step, object contours are divided into separate contour segments. In the segment grouping step, contour evidences are built by joining the contour segments that belong to the same object. Once the contour evidence is obtained, contour estimation is performed using numerically stable direct ellipse fitting.

This method consists of two consecutive main step (Figure 19): contour evidence extraction and contour estimation. the segmentation process starts with pre-processing to build an image silhouette and the corresponding edge map, the edge map is constructed from output of last watershed stage using the Canny edge detector, In the contour evidence extraction steps, edge points that belonged to each object are grouped using concave points and properties of fitted ellipses. Once the contour evidence has been obtained, contour estimation is carried out to infer the missing parts of the overlapping objects.

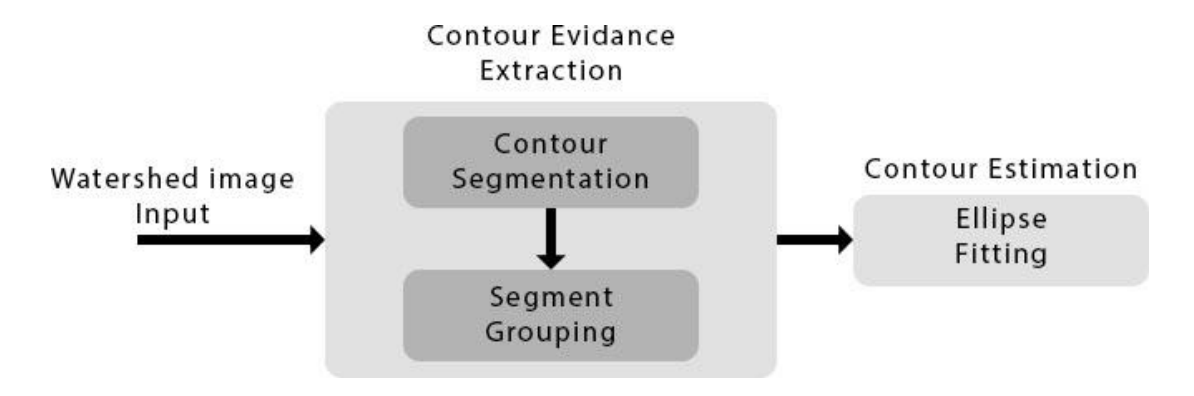


Figure 20 Concave Point segmentation Algorithm.

4.4.3.1 Contour Evidence Extraction

The first step is to extract the contour evidence containing the visible parts of the objects boundaries that can be used to inference the occluded parts of overlapped objects. The contour evidence extraction involves two separate tasks: contour segmentation and segment grouping.

4.4.3.1.1 Contour Segmentation

A partial overlap between two or more elliptic-shape objects leads to a concave shape with concave edge points that correspond to the intersections of the object boundaries. It is a common practice to utilize these concave points to segment the contour of overlapping objects [67]. Different methods such as polygonal approximation, curvature, and angle have been applied to determine the location of concave points in the image. In this work, after extracting the image edge by canny edge detector, the concave points are obtained through the detection of corner points followed by the concavity test [67]. The corner points are detected using the modified curvature scale space (CSS) method based on curvature analysis [67]. The output of the corner detector includes the points with the maximum curvature lying on both concave and convex regions of object contours. Since being only interested in the concave points joining the contours of overlapping objects, the detected corner points are examined if they lie on concave regions. Let us denote a detected corner point by pi, and its two kth adjacent contour points by p_{i-k} and p_{i+k} . The corner point pi is qualified as concave if the line connecting p_{i-k} to p_{i+k} does not reside inside the object. The obtained concave points are used to split the contours into contour segments. Figure 20 shows an example of concave point extraction and contour segmentation.

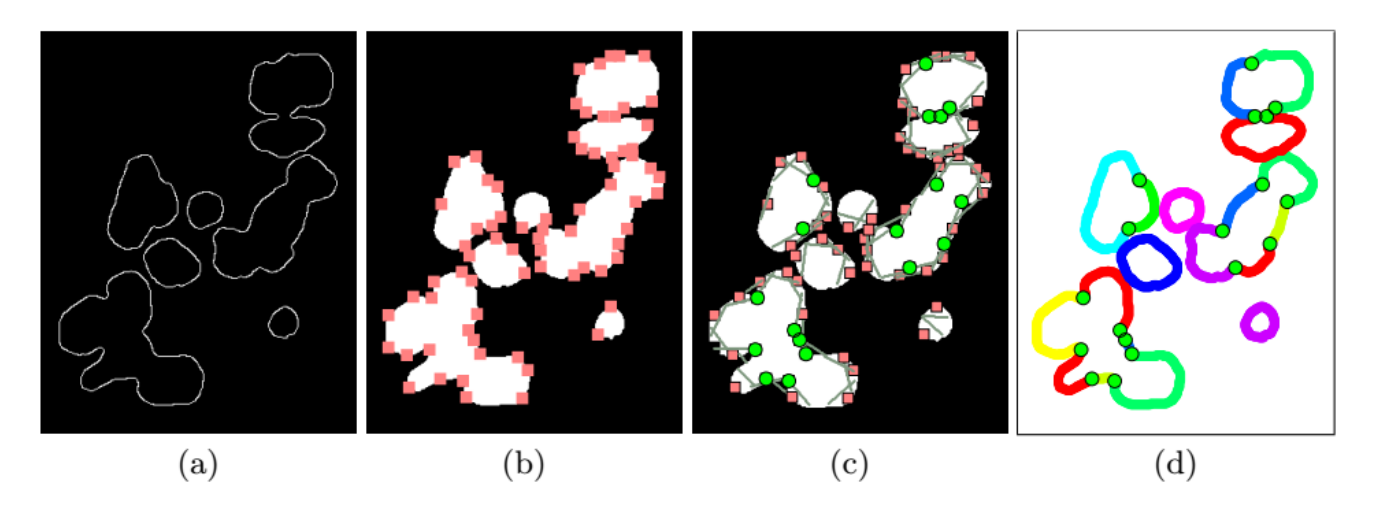


Figure 21 Contour segmentation: (a) Edge map; (b) Corner detection; c) Concavity test to extract concave corners (green circle) and removed convex corners (pink square); (d) Contour segmentation by concave points the colors are used only for illustrative.

4.4.3.1.2 Segment Grouping

Due to the overlap between the objects and the irregularities in the object shapes, a single object may produce multiple contour segments. Segment grouping is needed to merge all the contour segments belonging to the same object. The basic idea behind the proposed method for segment grouping is to find a group of contour segments that together form an object with elliptical shape. Segment grouping in its naive form, iterates over each pair of contour segment, examining if they can be combined. In this work, to optimize the grouping process, a limited search space is applied and the contour segment under grouping process is only examined with the neighboring segments. Two segments are neighbor if the Euclidean distance between their center points is less than the predefine threshold value. The contour segment grouping is carried out through the process of ellipse fitting. Given a pair of contour segments, si and sj, and a function measuring the goodness of ellipse fitting, the segment si is grouped to sj if the goodness of ellipse fitted to the joint segments is higher compared to the goodness of ellipses fitted to each individual contour segments separately. The goodness of fit is described as average distance deviation (ADD) [68] which measures the discrepancy between the fitted curve and the candidate contour points. The lower value of ADD indicates higher goodness of fit and, therefore the joint rule to perform segment grouping in terms of ADD is defined as

$$ADD_{S_i \cup S_j} \le ADD_{S_i},$$

$$ADD_{S_i \cup S_j} \le ADD_{S_j}$$
(14)

Where the definition of ADD is as follows: Given the contour segment s_i consisting of n points, $S_i = \{p_k(x_k, y_k)_{k=1}^n$, and the corresponding fitted ellipse points, $S_{f,i} = \{p_{f,k}(x_{f,k}, y_{f,k})_{k=1}^n, ADD_{S_i} \text{ is defined as:} \}$

$$ADD_{S_i} = \frac{1}{n} \sum_{k=1}^{n} \sqrt{(x_k - x_{f,k})^2 + (y_k - y_{f,k})^2}$$
 (15)

Within the transformed coordinate system

$$\begin{bmatrix} x_k' \\ y_k' \end{bmatrix} = \begin{bmatrix} \cos \emptyset & -\sin \emptyset \\ \sin \emptyset & \cos \emptyset \end{bmatrix} \begin{bmatrix} x_k & -x_{eo} \\ y_k & -y_{eo} \end{bmatrix}$$
 (16)

Eq. (2) can be simplified to

$$ADD_{S_i} = \frac{1}{n} \left[\sum_{k=1}^{n} \sqrt{x'_k^2 + y'_k^2 (1 - \frac{1}{|D_k|})} \right]$$
 (17)

where D_k is given by

$$D_k^2 = \frac{{x'}_k^2}{a^2} + \frac{{y'}_k^2}{h^2} \tag{18}$$

And a, b, (x_{eo}, y_{eo}) and θ are the ellipse parameters, the semi-major axis length, the semi-minor axis length, the ellipse center point, and the ellipse orientation angle with respect to x axis, respectively.

The plain ADD criterion for segment grouping often leads to undesired results if the contour points do not strictly fit to the ellipse model. In order to address this issue, additional rules are needed. Given a pair of contour segments to be processed for grouping, the segment with longer length usually provides a more reliable clue to the object than the shorter one.

Based on this assumption, a weighing scheme using the length of contour segments is added to the grouping process where the ADD of contour segment with longer length is downweighted by the ratio of its length with respect to the total length of contour segments to be grouped. Assuming the contour segment si is longer than contour segment s_j , Eq. (14) is replaced by

$$ADD_{S_i \cup S_j} \le \omega_i ADD_{S_i},$$

$$ADD_{S_i \cup S_j} \le ADD_{S_j}$$
(19)

Where

$$\omega_i = \frac{l_i}{l_i + l_i} \tag{20}$$

and li and lj are the lengths of contour segments s_i and s_j , respectively. The contour segments in far proximity are less likely to represent a single object and should not be merged. As the result, the two contour segments whose ellipse models are at very far distance from each other should not grouped. Either, ellipse fitted to the combined contour segments should not be at far distance from the ellipses fitted to each individual contour segments. Following these conventions and being interested in grouping of close contour segments, two additional rules are applied similarly to [10]. Let us denote the centroids of the fitted ellipse for the contour segments s_i , s_j and $s_i c_j$ by e_i , e_j and $e_i c_j$, respectively. The contour segments s_i and s_j

should not be grouped as a single segment provided that, first, the distance from the ellipse centroid of the combined contour segments $e_i u_j$ to the center of its members, e_i and e_j , is larger than the preset threshold t_I :

$$d(e_i, e_{ij}) > t_1$$

$$d(e_j, e_{ij}) > t_1$$
(21)

and second, the distance between their corresponding ellipse centroids is larger than the predefined threshold t_2

$$d(e_i, e_j) > t_2 \tag{22}$$

Where $d(p_1, p_2)$ is the Euclidean distance between points p_1 and p_2 .

The value of t1 can be determined using the object properties [69] and is usually close to the length of the minor axis of fitted ellipses to the smallest object in the image. The value of t2 should be set in such way that prevents the grouping of the contour segment belong to different objects or as [69] proposed 2.5 to 4 times higher than the threshold t_1 . Figure 21 shows an example of segment grouping.

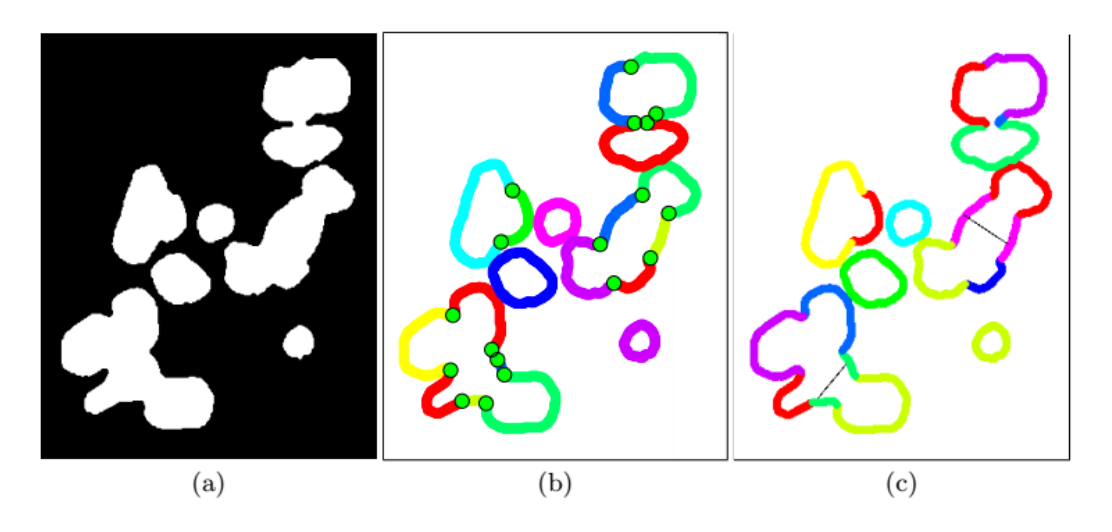


Figure 22 Segment grouping: (a) Original binary image; (b) Contour segmentation; (c) Segment grouping (the thin gray lines are added to illustrate the grouping of non-adjacent segments).

4.4.3.2 Contour Estimation

The last step of proposed method is the contour estimation, where, by means of the visual information produced from the previous step, the missing parts of the object contours are estimated. Ellipse fitting is a very common approach in overlapping object segmentation, especially in the medical and industrial applications. The most efficient recent ellipse fitting methods based on shape boundary points are generally addressed through the classic least square fitting problem. In this work, the contour estimation is addressed through a stable direct least square fitting method [70] where the partially observed objects are modeled in the form of ellipse-shape objects. Figure 22 shows an example of contour estimation applied to contour evidences.

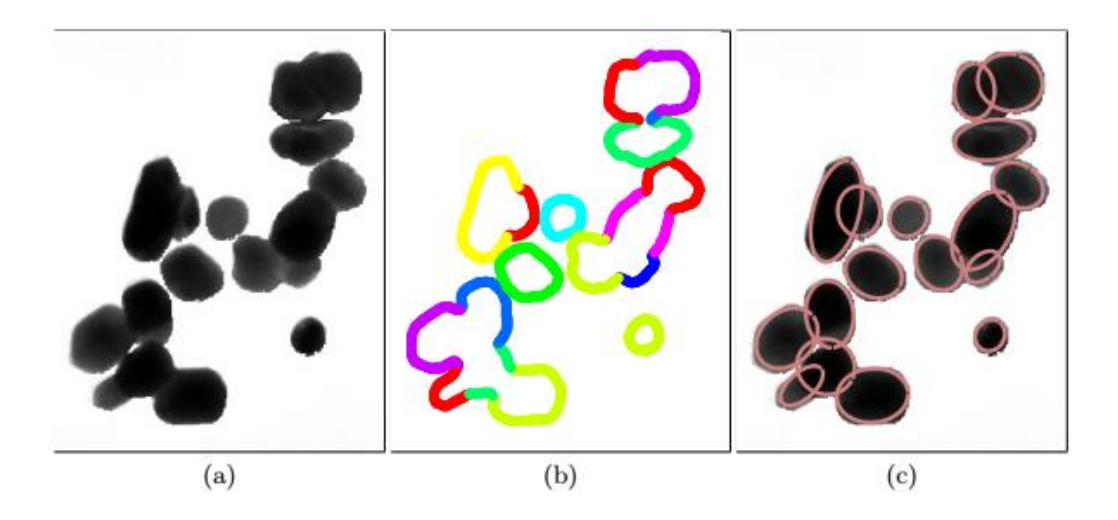


Figure 23 Contour estimation: (a) Original image; (b) Contour evidence extraction; (c) Contour estimation.

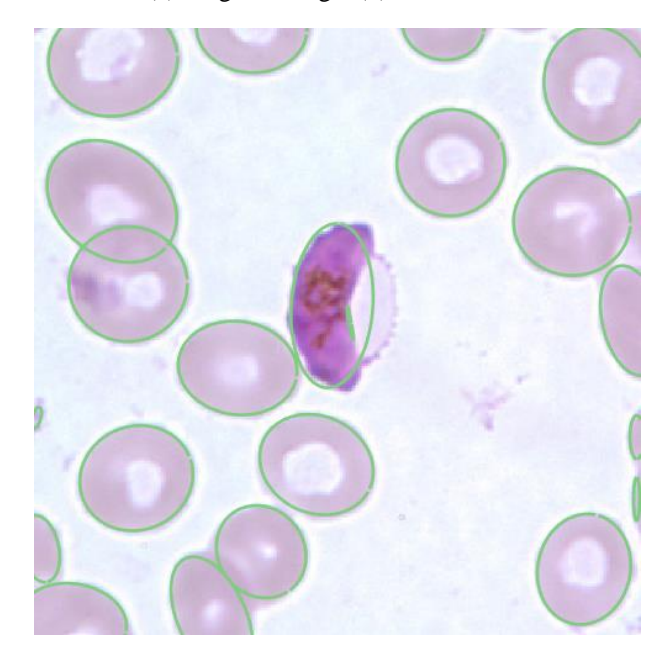


Figure 24 one of the test images segmented using concave point and ellipse fitting.

4.5 Feature Extraction

Recent researches on feature extraction and selection of red blood cell have shown the importance of feature extraction phase for red blood cell analysis. Researchers have used different features based on their target blood cells/disease. The features which give predominant difference between normal cells and infected cells are identified as feature set. Textural [71] and color features [72, 73] are very important in order to differentiate form other cells and has been widely used for blood cell recognition whereas color features play important

role in order to differentiate similar shapes and overlapped cells. a geometrical and intensity features along with GLCM based texture features was used.

4.5.1 Geometrical features

Geometrical features remain very important for complex shape recognition and lot of researchers used geometrical features for blood analysis. extracting geometrical features that are invariant under different condition and analogous to those used by hematologist. These features include nucleus area, relative area, nucleus parameter, nucleus relative parameter, nucleus roundness and nucleus relative roundness, nucleus mean, nucleus variance, cytoplasm area, cytoplasm parameter, cytoplasm mean, cytoplasm variance, cytoplasm ratio to nucleus and number of object of in nucleus. for leukocyte recognition, area, compactness and form factor feature was used.

$$Area(R) = Total\ Number\ of\ pixels(R)$$
 (23)

$$compactness(R) = \frac{2\sqrt{\pi Area(R)}}{perimeter(R)}$$
 (24)

$$form \ factor(R) = \frac{4\pi Area(R)}{perimeter^2}$$
 (25)

4.5.2 Texture Features

Due to the importance of textural feature for complex object classification, we have extracted several texture features, i.e. co-occurrence matrix. The co-occurrence feature matrix describes the second order probabilistic features relating to the gray level relationship in the pixel neighborhood. GLCM is statistical measure used to characterize the image texture by calculating how often pairs of pixel occurrence in special specified relationship. It is a symmetric matrix constructed on the basis of image gray levels with distance and angle. The disparate co-occurrence feature matrix is created by the divergence of angle and distance. As different type of nucleus represents different texture, thus GLCM based texture features are taken into account for classification. If an image M consists of N gray levels, the co-occurrence matrix dimension is NxN. Let I be the segmented region of the leukocyte nuclei, the GLCM is

computed by summing all the texture information in image I including the average spatial relationship between neighboring gray tones.

six texture features were used from co-occurrence matrix alongside statistical features to represent mean, skewness, kurtosis, standard deviation, dissimilarity and Inverse Difference Moment. Co-occurrence feature matrix is computed as

$$C_{\Delta x, \Delta y}(i, j) = \sum_{x=1}^{n} \sum_{y=1}^{m} \begin{cases} 1 & \text{if } I(x, y) = i \ I(x + \Delta x, y + \Delta y) = j \\ 0 & \text{Otherwise} \end{cases}$$
(26)

Dissimilarity

$$\frac{1}{2} \sum_{i=1}^{N} \left| \frac{b_i}{B} - \frac{w_i}{W} \right| \tag{27}$$

Inverse Difference Moment

$$IDM = \sum_{i=0}^{G-1} \sum_{j=0}^{G-1} \frac{1}{1 + (i-j)^2} P(i,j)$$
 (28)

Mean

$$M1(k,l) = \frac{1}{NR} \sum_{m \in R} \sum [u(m-k, n-l)]$$
 (29)

Skewness

$$M5(k,l) = \frac{1}{NR} \sum_{mn \in R} \sum [u(m-k, n-l) - Ml(k,l)]$$
(30)

Kurtosis

$$M6(k,l) = \frac{1}{NR} \sum_{mn \in R} \sum [u(m-k,n-l) - M1(k,l)]$$
(31)

Standard deviation

$$M3(k,l) = \sqrt{\frac{1}{NR} \sum_{mn \in R} \sum_{mn \in R} [u(m-k, n-l) - M1(k, l)]}_{2}$$
(32)

4.6 Classification of infected cells

Conventional approaches of pattern classification involve clustering training samples and associating clusters to given categories. The complexity and limitations of previous mechanisms are largely due to the lacking of an effective way of defining the boundaries among clusters. This problem becomes more intractable when the number of features used for classification increases [74].

The neuro-fuzzy approach is better than neural network classifiers in the sense that prior knowledge about the training data set can be encoded into the parameters of the neuro-fuzzy classifier. This encoded knowledge, usually acquired from human experts or data visualization techniques, can almost always allow the learning process to begin from a good initial point not far away from the optimal one in the parameter space, thus speeding up the convergence to the optimal or a near-optimal point. Moreover, the parameters obtained after the learning process can be easily transformed into structure knowledge in the form of fuzzy if-then rules [74].

Generally, ANFIS is used as classifier. ANFIS is a function approximator program. But, the usage of ANFIS for classifications is unfavorable. For example, there are three classes, and labeled as 1, 2 and 3. The ANFIS outputs are not integer. For that reason, the ANFIS outputs are rounded, and determined the class labels. But, sometimes, ANFIS can give 0 or 4 class labels. These situations are not accepted. As a result, ANFIS is not suitable for classification problems.

By using the k-means algorithm to initialize the fuzzy rules. For that reason, a number of two clusters were chosen (infected and non-infected). Also, Gaussian membership function is only used for fuzzy set descriptions, because of its simple derivative expressions the differences are about the rule weights and parameter optimization. The rule weights are adapted by the number of rule samples. The scaled conjugate gradient (SCG) algorithm is used to determine the optimum values of nonlinear parameters. The SCG is faster than the steepest

descent and some second order derivative based methods, then Linguistic hedges are applied to the fuzzy sets of rules, and are adapted by SCG algorithm. By this way, some distinctive features are emphasized by power values, and some irrelevant features are damped with power values. The power effects in any feature are generally different for different classes. The using of linguistic hedges increases the recognition rates [75].

The database used for training were acquired from the central Disease control CDC which include 145 malaria image.

After segmentation process, every segmented cell was treated individually, resulting in 2259 training cells.

The training and testing recognition rates were 96.33% and 96.31%.

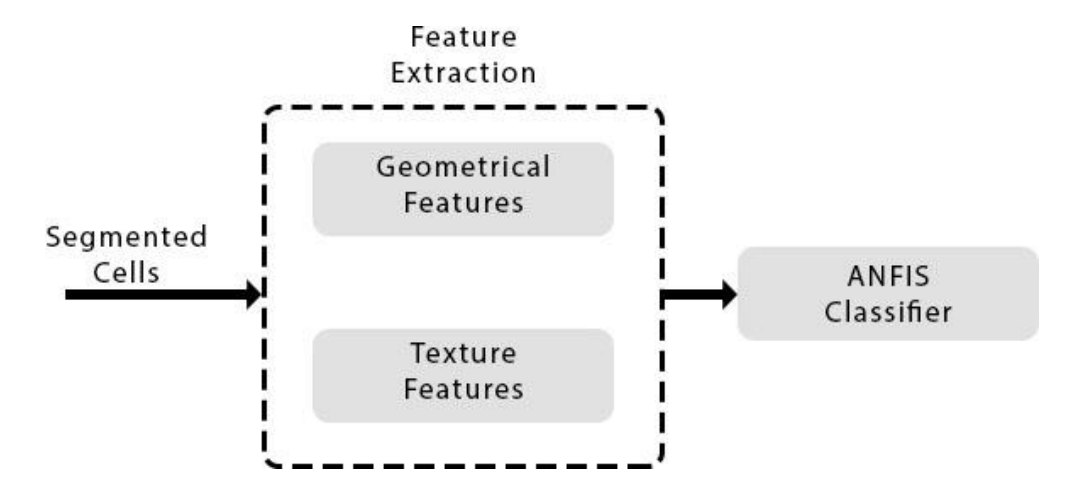


Figure 25 Feature Extraction and Classification workflow

Results and discussions

5.1 Results

After training ANFIS classifier, it shows 96.33% and 96.31% recognition rates for both training and testing. Figure 25 address the classifier performance with 1500 iteration.

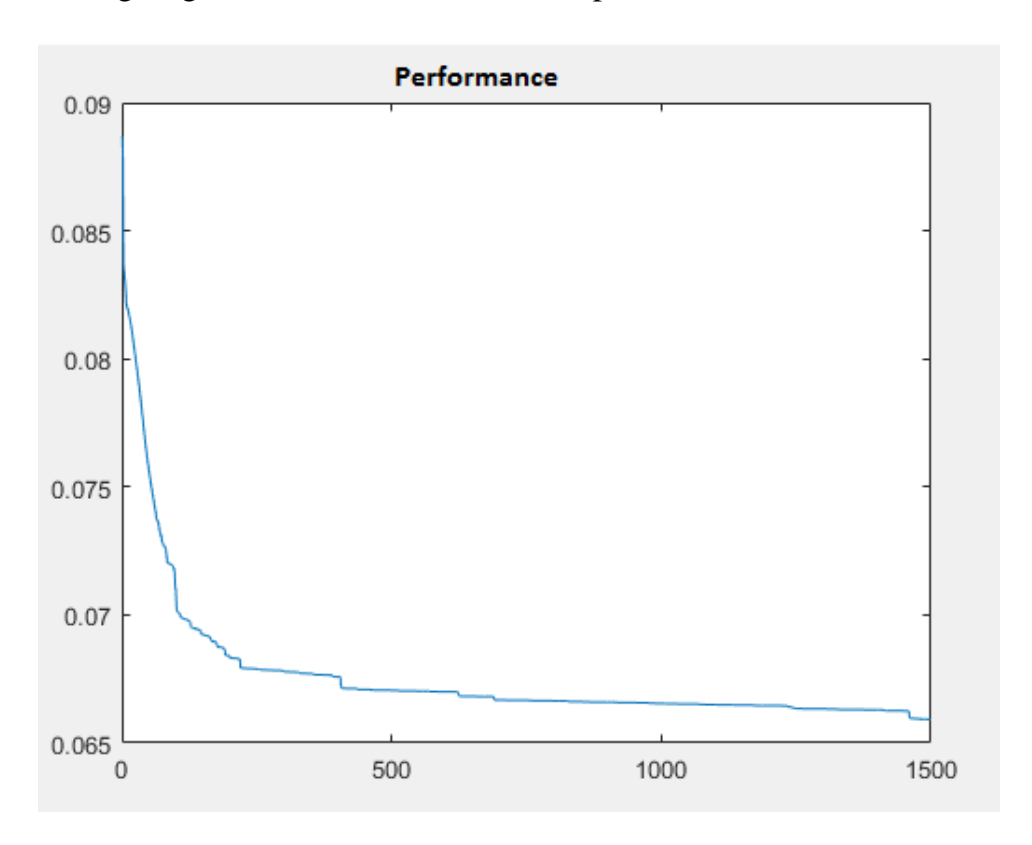


Figure 26 ANFIS classifier Performance

The main Classification function is AMCC in matlab which accepts three inputs: first is the blood smear image (colored), second is the minimum cell radius, third is the maximum cell radius. This limits ellipse estimation result to RBCs size range. Finally, the results of classification are: first statistical Result, which gives the total count of RBCs, normal RBCs count and infected RBCs count. Second, an image which labels infected RBCs with Red color and normal RBCs in green color which is shown in Figure 27.

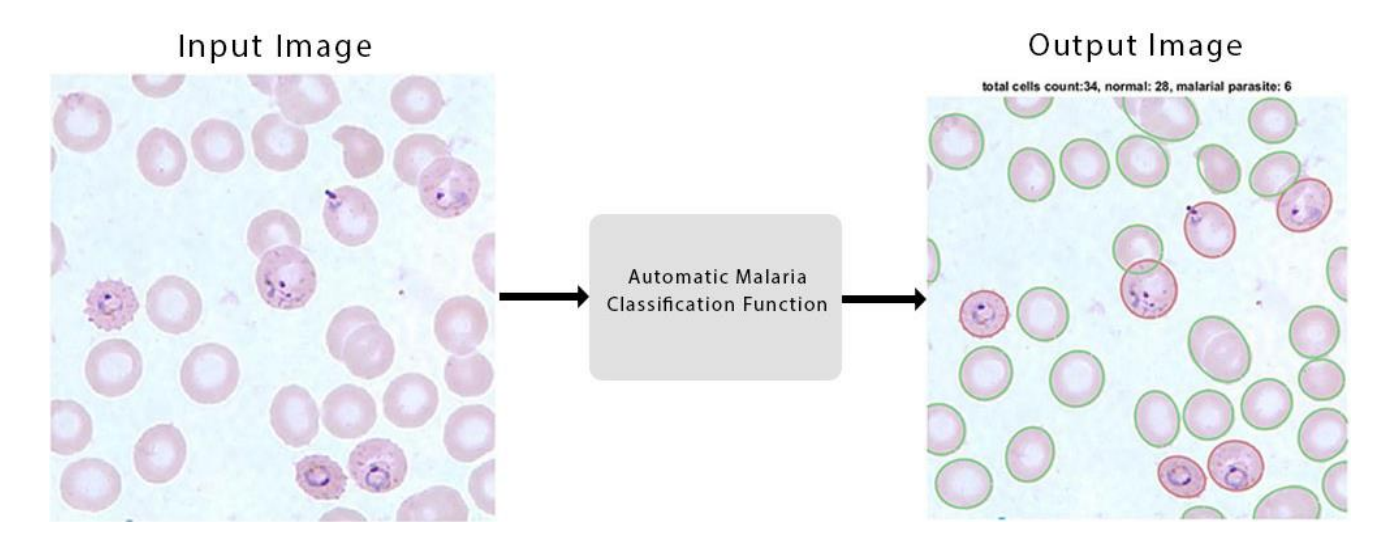


Figure 27 Automatic malaria classification function and its input and output (Green normal, red infected malaria cells).

Figure 28 shows the graphical user interface which implements AMCC function to a user-friendly environment which enables the technician to choose a stored blood image, shows its size and color type information, selecting RBCs size range. finally, analyze the image to classify RBCs and gives statistical result in the bottom of the window labeled as count, blood image diagnosis as positive or negative and last labeling input image with green color for normal RBCs and red color for infected RBCs with malaria cells.

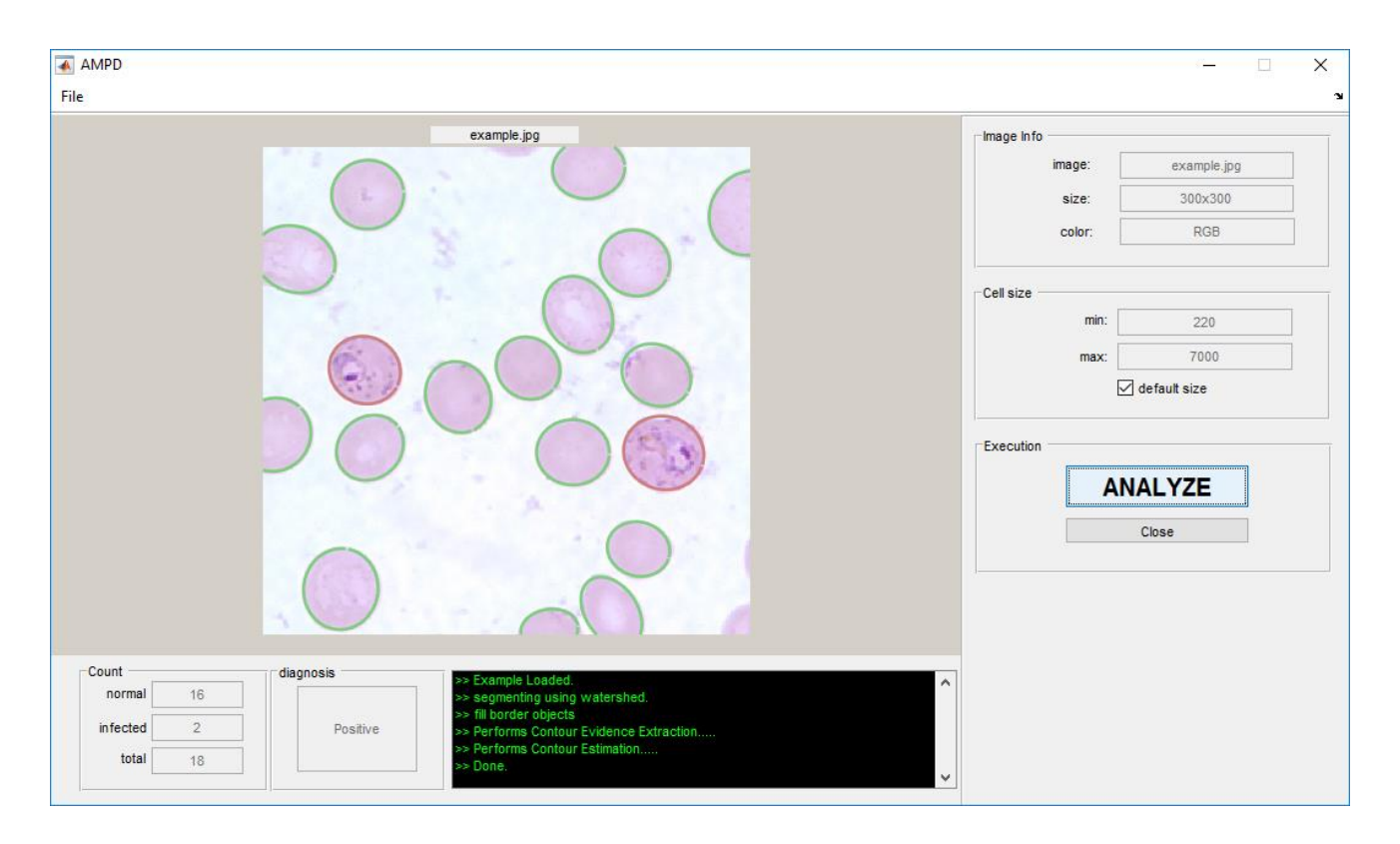


Figure 28 graphical user interface program.

A number of 27 infected test images acquired from Khartoum laboratory administration, Table 2 shows manual (reference) cells count, number of infected cell and normal cells and compare it with the proposed method results.

Table 2 Comparison between manual and automated method

	Manual Reference			Autom	atic Metho	d
Images	total number	normal	malaria	total number of	normal	malaria
number	of cell	cells	cells	cell	cells	cells
1	30	24	6	29	21	8
2	18	17	1	18	17	1
3	51	44	7	52	45	7
4	47	38	8	37	29	8
5	18	16	2	18	16	2
6	34	28	6	34	28	6
7	30	28	2	30	28	2
8	25	17	8	25	21	4
9	29	24	5	30	25	5
10	35	32	3	35	32	3
11	17	15	2	17	16	1
12	17	15	2	20	18	2
13	14	13	1	15	14	1
14	7	4	3	7	4	3
15	13	12	1	13	12	1
16	36	35	1	36	34	2
17	15	14	1	16	14	2
18	18	16	2	16	14	2
19	39	37	2	34	30	4
20	13	12	1	14	13	1
21	48	46	2	48	46	2
22	21	17	4	24	20	4
23	14	13	1	16	15	1
24	15	12	3	17	15	2
25	63	60	3	59	56	3
26	19	17	2	19	17	2
27	13	11	2	13	11	2

Table 3 Detection error analysis

Result Type	Mean error	Stander deviation	Error Range
Total cells mean	1.3703	2.203985	+-10
Detection Error			
Normal cells mean error	1.7037	2.267068843	+-7
Infected cells mean error	0.445	0.933699562	+-4

The 27 images have a total of 699 cell, 617 are normal and 81 are infected. The system detects a total of 692 cells, 611 are normal and 81 are infected with malaria.

Mean rate of 98.9% total rate of detection, 99% detection rate of normal cells and 100% detection rate for infected cells.

5.2 Discussions

The results indicate that image analysis may be used for the automatic classification of infected blood cells from patients with malaria cell anemia the pattern classes of normal and other infected. Most of the previous methods which were being used for Malaria classification are time consuming and expensive. Pathologist's skill has an important role in the results accuracy, respect to all of these facts, the several excluded results would have no coordination with each other. May be for a same sample, two pathologists give different opinion on diagnosis. In the proposed method cells, unique features are used for diagnosis, morphological (shape based features) and textural features which allow to get quantitative results. This is so useful for the pathologists to authorizes him/her to decide in many aspects. But in many works these values were comparative and were not available for pathologist because they were not real and numeral data. Finally, this method provides us with fast, quantitative results which are not as expensive as the previous ones.

Conclusion & recommendations

6.1 Conclusion

There are different methods for malaria parasite detection. The proposed automated algorithm has many advantages compared to other diagnostic techniques. It avoids the problems associated with rapid methods, such as being species-specific and having high pertest costs, while retaining many of the traditional advantages of microscopy, example. species differentiation.

This Thesis addresses the classification of malaria diseases using image processing. Although, malaria cell segmentation and morphological analysis is a challenging problem due to both the complex cell nature uncertainty in microscopic videos. by effectively analyzing various parameter of blood cell image using GLCM matrix as Texture features and Geometrical feature. The experimental results indicate that the proposed approach is a valuable approach, which can be significantly support an accurate identification of malaria diseases in a little computational effort. There can be mistake in counting manually the number of RBC & WBC (process of Giemsa) as the boundaries are not clearly defined or visible which lead us to the error in wrong decision. So, to solve this problem the developed algorithm can be more helpful for other techniques. As this system, can meet the real-time application requirements, so a standalone working version of this system can be developed.

6.2 Recommendations

The performance of the system can be increased by creating new set of feature which can be well optimized with classifier and which gives best, also training ANFIS classifier using newly developed particle swarm optimization (PSO) algorithm should increase system's detection rate significantly to obtain better results. finally developing new technique instead of ellipse fitting method to trace and simulate overlapped cells boundaries.

References

- [1] World Health Organization. What is malaria? Facts Sheet no 94. http://www.who.int/mediacentre/factsheets/fs094/en/.
- [2] Rafael, M. E., Taylor, T., Magill, A., Lim, Y., Girosi, F., Allan, R. (2006). Reducing the burden of childhood malaria in Africa: the role of improved diagnostics. Nature. pp. 39-48.
- [3] Tangpukdee, N., Duangdee, C., Wilairatana, P., Krudsood, S. (2009). Malaria Diagnosis: A Brief Review. Korean Journal of Parasitology. pp. 93-102.
- [4] Reyburn, H., Mbatia, R., Drakeley, C., Carneiro, I., Mwakasungula, E., Mwerinde, O., Saganda, K., Shao, J., Kitua, A., Olomi, R., Greenwood, B. M., Whitty, C. J. M. (2004). Over diagnosis of malaria in patients with severe febrile illness in Tanzania: a prospective study. *British Medical Journal*. **329**(7476).
- [5] Chandra, U., Bahendwar, Y. (2015). "Detection of Malaria Disease through Soft Computing", IJARCSSE Volume-5, Issue-10,
- [6] Makler, M., Palmer, C., Alger, A. (1998). A Review of Practical Techniques for the Diagnosis of Malaria. Ann Trop Med Parasitol 92(4). pp. 419-433.
- [7] National Institute of Allergy and Infectious Diseases. (2012). Life Cycle of the Malaria Parasite. National Institutes of Health.
- [8] Centers for Disease Control and Prevention (2010). Diagnostic Findings: Malaria. CDC Center for Global Health.
- [9] Ogunbajo, A. (2011). Migration of Plasmodium Sporozoites through Host Cells. Journal of the Student National Medical Association.
- [10] Guyton, A., Hall, J. (2011). Textbook of Medical Physiology. 12th ed. Philadelphia, PA: Elsevier. Print.
- [11] Jones, C.S., Mayfield, S.P. (2012). Steps toward a globally available malaria vaccine: Harnessing the potential of algae for future low cost vaccines. Bioengineered. 4(3)
- [12] Michalakis, Y., Renaud, F. (2009). Evolution in vector control. Nature. pp. 298-300.
- [13] Maxmen, A. (2012). Malaria plan under scrutiny. Nature. pp. 13-14
- [14] Maxmen, A. (2012). Malaria surge feared. Nature. pp.485: 293.
- [15] Centers for Disease Control and Prevention. (2010). Malaria Treatment (United States). Centers for Disease Control.
- [16] World Health Organization. (2009). "Online Q&A." http://www.who.int/features/qa/26/en/index.html.
- [17] Williams, I. (2013). Drug-resistant malaria in Thailand threatens deadly global 'nightmare'. NBC News. http://tinyurl.com/aqwug3e.
- [18] Bill and Melinda Gates Foundation. (2011). Malaria Strategy Overview. http://www.gatesfoundation.org/malaria/Documents/malaria-strategy.pdf.
- [19] Wilson, M. L. (2012). Malaria Rapid Diagnostic Tests. Medical Microbiology. dpp. 1637-1641.
- [20] Centers for Disease Control and Prevention. (2011a). "Guidelines for Treatment of Malaria in the United States." Centers for Disease Control. http://www.cdc.gov/malaria/resources/pdf/treatmenttable.pdf
- [21] Centers for Disease Control and Prevention. (2011). "Treatment of Malaria (Guidelines for Clinicians)." Centers for Disease Control. Available at: http://www.cdc.gov/malaria/resources/pdf/clinicalguidance.pdf.

- [22] Tek, F. B., Dempster, A. G., Kale, I. (2009). Computer Vision for Microscopy Diagnosis of Malaria. Malaria Journal. pp. 153.
- [23] Adeoye, G. O., Nga, I. C. (2007). Comparison of Quantitative Buffy Coat technique (QBC) with Giemsa-stained thick film (GTF) for diagnosis of malaria. Parasitology International. pp. 308-312.
- [24] Payne, D. (1988). Use and limitations of light microscopy for diagnosing malaria at the primary health care level. Bulletin of the World Health Organization. pp. 621-626.
- [25] Sanofi, A. (2002). Artifacts commonly mistaken for malaria parasites. Available at: http://www.impact-malaria.com/web/malaria training/identification species/artefacts
- [26] Keiser, J., Utzinger, J., Premji, Z., Yamagata, Y., Singer, B. H. (2002). Acridine Orange for malaria diagnosis: its diagnostics performance, its promotion and implementation in Tanzania, and the implications for malaria control. Annals of Tropical Medicine & Parasitology. pp. 643-654.
- [27] Kawamoto, F., Billingsley, P. F. (1992). Rapid Diagnosis of Malaria by Fluorescence Microscopy. Lancet. pp. 200-202.
- [28] QBC Diagnostics. (2012). QBC Malaria Test: Frequently Asked Questions (FAQs). QBC Diagnostics. Available at: http://www.qbcdiagnostics.com/products/fm/malaria/faq.asp#f10
- [29] Estacio, R. H., Dy, E. E. R., Cresswell, S., Coronel, R. F., Alora, A. T. (1993). The Quantitative Buffy Coat Technique (QBC) in Early Diagnosis of Malaria: The Santo Tomas University Hospital Experience. Philippine Journal of Microbiology and Infectious Disease. 22(2).
- [30] Levine, R. A., Wardlaw, S. C., Patton, C. L. (1989). Detection of hematoparasites using quantitative buffy coat analysis tubes. Parasitology Today. pp. 132-134.
- [31] Moody, A. (2002). Rapid Diagnostic Tests for Malaria Parasites. Clinical Microbiology Reviews. 15(1): 66-78.
- [32] Jang S. (1993). Adaptive network-based Fuzzy Inference System. IEEE Journal, Vol.23, No.3, PP.665-685, ISSN 0018-9472
- [33] Jang, S.; Sun T. & Mizutani E. (1997). Neuro-Fuzzy and Soft Computing a Computational Approach to Learning and Machine intelligence, Prentice Hall, Inc. ISBN 0132610663
- [34] Fuzzy Logic Toolbox User's Guide for Use with MATLAB (2009).
- [35] Zaho, J. & Bose, B. (2002). Evaluation of membership Functions for Fuzzy Logic Controlled Induction Motor Drive. IEEE Journal, Vo.1, No.pp.229-234, ISBN 0-7803-7474-6. S
- [36] Lin. C. & Lee. C. (1996). Neural Fuzzy Systems-A Neuro Fuzzy Synergism to Intelligent Systems. Prentice Hall P T R. Upper Saddle River, N.J., ISBN 0-13-235169-2
- [37] Mamdani, E. and Assilian, S. (1975). An experiment in linguistic synthesis with a fuzzy logic controller. International Journal of Man Machine Studies, Vol.7, No.1, pp. 1-13, ISSN 00207373
- [38] Sugeno, M. (1985). Industrial applications of fuzzy control, Elsevier Science Pub, ISBN0444878297, NY, USA
- [39] Hamidian D. & Seyedpoor M. (2010). Shape Optimal Design of Arch Dams Using an Adaptive Neuro-Fuzzy Inference System and Improved Particle Swarm Optimization. Jornal of Applied Mathematical Modelling. Vol.34, No.6. pp.1574-1585.
- [40] Memeu D., Kaduki, K., Mjomba, A., Muriuki, N., Gitonga, L. (2013). Detection of plasmodium parasites from images of thin blood smears, Open Journal of Clinical Diagnostics. pp.183-194.
- [41] Gitonga, L., Memeu, D., Kaduki, K., Kale, M., Muriuki, N. (2014). Determination of Plasmodium Parasite Life Stages and Species in Images of Thin Blood Smears Using Artificial Neural Network, Open Journal of Clinical Diagnostics. pp. 78-88.

- [42] Veluchamy, M., Perumal, K. and Ponuchamy, T. (2012). Feature Extraction and Classification of Blood Cells Using Artificial Neural Network. American Journal of Applied Sciences 98, ISSN 1546-9239. pp.615-619
- [43] Dipti D. (2013). Exploring the use of Artificial Neural Network and Bayesian Network for Malaria Detection, Sixth IRAJ International Conference. ISBN: 978-93-82702-32- 0, pp.24-27
- [44] Chawla, P., Mittal, R., Grewal, K. (2012). Hybrid Filtering Technique for Image Denoising Using Artificial Neural Network, IJEAT Volume-1, Issue-3.
- [45] Mishra, S., Panda, G., Meher, G. (2009). Chebyshev Functional Link Artificial Neural Networks for Denoising of Image Corrupted by Salt and Pepper Noise. International Journal of Recent Trends in Engineering, Vol. 1, No.1.
- [46] Yazeed A. (2012). Artificial Neural Networks Evaluation as an Image Denoising Tool, IDOSI Publications.
- [47] Sarangi, S., Sarangi, S., Sarangi, S. (2014). Performance Analysis of Filter based on Functional Link Artificial Neural Network, IJCA, Volume 93 No 1.
- [48] JunyuanXie, LinliXu, Chen, E. (2012) Image Denoising and Inpainting with Deep Neural Networks, Advances in Neural Information Processing Systems 25. pp.1-9.
- [49] Mohanty S. and Paramita P. (2014). Image Denoising Using Adaptive Filter Based on Computational Efficient Modified Functional Link Artificial Neural Network. SPC ERA IJSTE Vol-1, No-1.
- [50] Mastake A., Yongjia, C., Masato, K., QinyuZhang, Y. (2007). Additive and multiplicative noise reduction by back propagation neural Internationale, Lyon. France.
- [51] Yan, L., Wang, L., HuiYap K. (2004). A noisy chaotic neural network approach to image denoising" International Conference on Image Processing (ICIP). pp:1229-1232.
- [52] Marwaha, S., Monga, H., Shelza, (2012). Automatic Diagnosis Systems Using Image Processing-A Systematic Study", International Journal of Computer Science and Information Technology & Security (IJCSITS), ISSN: 2249-9555Vol. 2, No.2. pp.388-391.
- [53] Ms. Deepali Ghate, Mrs.Chaya, C. Dr. N Usha Rani, "automatic detection of malaria parasite from blood images", International journal of advanced computer technology | Volume 4, Number 1, ISSN:2319-7900, pp.129-132.
- [54] Savkare S. and Narote S. (2011). Automatic Detection of Malaria Parasites for Estimating Parasitemia. International Journal of Computer Science and Security (IJCSS), Volume (5): Issue (3). pp. 310-315.
- [55] Suradkar P. (2013). Detection of Malarial Parasite in Blood Using Image Processing. International Journal of Engineering and Innovative Technology (IJEIT)Volume 2, Issue 10. pp:124-126.
- [56] Shiff, C., (2002). Integrated approach for malaria control. Clin. Microbiol. Rev.15, pp.278–293.
- [57] Kumar, A., Choudhary A., Tembhare P., Pote C. (2012). Enhanced Identification of Malarial Infected Objects using Otsu Algorithm from Thin Smear Digital Images, International Journal of Latest Research in Science and Technology Vol.1, Issue 2: Page No159-163.
- [58] Makkapati, V., and Rao, R. (2009) Segmentation of malaria parasites in peripheral blood smear images., Proceedings of IEEE International Conference on Acoustics, Speech and Signal Processing, ICASSP 2009, pp. 1361-1364.
- [59] Raviraja, S., Bajpai, G., Sharma, S. (2007). Analysis of Detecting the Malaria Parasite Infected Blood Images Using Statistical Based Approach IFMBE Proceedings, 3rd Kuala Lumpur International Conference on Biomedical Engineering 2006, vol. 15, part 12, pp. 502-505.

- [60] Ruberto C., Dempster, A., Khan S., Jarra, B. (2000). Segmentation of blood images using morphological operators., Proceedings of 15th International Conference on Pattern Recognition Barcelona, Spain, vol. 3, pp. 3401.
- [61] Díaz, G., Gonzalez, F., Romero, E. (2007). Infected cell identification in thin blood images based on color pixel classification: Comparison and analysis. Lecture Notes in Computer Science 4756, 812.
- [62] Otsu, N. (1979). A threshold selection method from gray-level histograms. IEEE Trans. Sys., Man., Cyber. 9 (1): 62–66. doi:10.1109/TSMC.1979.4310076.
- [63] Najman, L. and Schmitt, M. (1994). Watershed of a continuous function. In Signal Processing (Special issue on Mathematical Morphology.), Vol. 38. p. 99–112
- [64] Park, C., Huang, J.Z., Ji, J.X., Ding, Y. (2013). Segmentation, inference and classification of partially overlapping nanoparticles. IEEE Transactions on Pattern Analysis and Machine Intelligence 35, pp.669–681
- [65] Zhang, W.H., Jiang, X., Liu, Y.M. (2012). A method for recognizing overlapping elliptical bubbles in bubble image. Pattern Recognition Letters 33, pp.1543 1548
- [66] Kothari, S., Chaudry, Q., Wang, M. (2009). Automated cell counting and cluster segmentation using concavity detection and ellipse fitting techniques. In: IEEE International Symposium on Biomedical Imaging, pp.795–798
- [67] Zafari, S., Eerola, T., Sampo, J., Kälviäinen, H., & Haario, H. (2015, December). Segmentation of Partially Overlapping Nanoparticles Using Concave Points. In International Symposium on Visual Computing (pp. 187-197). Springer International Publishing
- [68] Zhang, W.H., Jiang, X., Liu, Y.M. (2012). A method for recognizing overlapping elliptical bubbles in bubble image. Pattern Recognition Letters 33, pp.1543 1548
- [69] Bai, X., Sun, C., Zhou, F. (2009). Splitting touching cells based on concave points and ellipse fitting. Pattern Recognition 42, pp.2434 2446
- [70] Fitzgibbon, A., Pilu, M., Fisher, R.B. (1999). Direct least square fitting of ellipses. IEEE Transactions on Pattern Analysis and Machine Intelligence 21, pp.476–480
- [71] Kumar, A., Choudhary, A., Tembhare, P., Pote, C. (2012). Enhanced identification of malarial infected objects using otsu algorithm from thin smear digital images. International Journal of Latest Research in Science and Technology ISSN (Online), pp.2278-5299, 1, 159.
- [72] Chen, T., YongZhang, Wang, C., ZhenshenQu, FeiWang, Mahmood T. (2013). Complex local phase based subjective surfaces (CLAPSS) and its application to DIC red blood cell image segmentation. Neurocomputing 99, 98.
- [73] Ahirwar, N., Pattnaik1, S., Acharya, B.(2012). Advanced image analysis based system for automatic detection and classification of malarial parasite in blood mages. International Journal of Information Technology and Knowledge Management 5, 59.
- [74] Sun CT, Jang JSR (1993). A neuro-fuzzy classifier and its applications. Proc. of IEEE

Appendix A

A.1 Matlab Codes:

A.1.1 Main function

```
function [ out, totCells,normCells, infecCells] = AMCC( inImage, opt )
%AMCC a function written by hosam hatim osman to classify and detect malarial
%parasite
  % load the method parameters
  if nargin < 2
    opt.show = 1;
    opt.minCellRadius = 220;
    opt.maxCellRadius = 7000;
  end
  load engine2
  param = readparam();
  out.decision = 'normal';
  cellsEllipse = mia_particles_segmentation(inImage,param);
  %
       showEllipse(inImage,cellsEllipse);
  selcCellsEllipse = cellThresh(cellsEllipse,opt.minCellRadius,opt.maxCellRadius);
  [features,out.outCellsEllipse] = calcCellFeatures(inImage,selcCellsEllipse);
  out.label = evalfis(features(:,engine2.featureIdx),engine2.fis)';
  out.label(out.label > 1.5) = 2;
```

```
out.label(out.label < 1.5) = 1;
  totCells = length(out.label);
  normCells = length(out.label(out.label == 1));
  infecCells = length(out.label(out.label == 2));
  if ~isempty(out.label == 2)
     out.decision = 'infected';
  end
  if opt.show == 1
    showResult(inImage,out.outCellsEllipse,out.label);
  end
end
function [feature,outCellsEllipse] = calcCellFeatures(img, cellsEllipse)
  if size(img, 3) == 3
    img = img(:,:,2);
  end
    i1 = rescale(morphRecon(img));
%
%
     o_pso = segmentation(i1,2,'pso');
%
     o_pso_bw = imfill(~im2bw(o_pso,graythresh(o_pso)),'holes');
  o_pso_bw = imfill(~im2bw(img,graythresh(img)),'holes');
```

```
sz = size(img);
  cnt = 0;
  outCellsEllipse = {};
  for i = 1:length(cellsEllipse)
    x = cellsEllipse{i}(:,1); y = cellsEllipse{i}(:,2);
    BW = o_pso_bw \& imdilate(poly2mask(x,y,sz(1),sz(2)),strel('disk',5));
    if ~isempty(find(BW, 1))
       cnt = cnt + 1;
       outCellsEllipse{cnt} = cellsEllipse{i};
       feature(cnt,:) = ftrCalc(img,BW)';
     end
  end
end
function showResult(inImage, CellsEllipse, label)
  imshow(inImage); hold on
  parasiteIdx = find(label == 2);
  normalIdx = find(label == 1);
  if ~isempty(CellsEllipse)
    if ~isempty(parasiteIdx)
       for iter=1:length(parasiteIdx)
```

```
plot(CellsEllipse{parasiteIdx(iter)}(:,1),CellsEllipse{parasiteIdx(iter)}(:,2),
'color',[0.8 0.5 0.5],'LineWidth', 2);
              end
           end
           if ~isempty(normalIdx)
              for iter=1:length(normalIdx)
                 plot(CellsEllipse{normalIdx(iter)}(:,1),CellsEllipse{normalIdx(iter)}(:,2),
'color',[0.5 0.8 0.5],'LineWidth', 2);
              end
           end
         end
         title(['total
                                           num2str(length(CellsEllipse))
                       cells
                                count:'
                                                                                  normal:
num2str(length(normalIdx)) ', malarial parasite: 'num2str(length(parasiteIdx))]);
       end
      function showEllipse(inImage, CellsEllipse)
         imshow(inImage); hold on
         if ~isempty(CellsEllipse)
           for iter=1:length(CellsEllipse)
              plot(CellsEllipse{iter}(:,1),CellsEllipse{iter}(:,2),
                                                                         'color',[0.5
                                                                                           0.8
0.5],'LineWidth', 2);
           end
```

end

end

A.1.2 morphological processing function

```
function [ out ] = morphRecon( img, strelSize)
%MORPHRECON Summary of this function goes here
% Detailed explanation goes here
if nargin < 2
    strelSize = 2;
end
se = strel('disk', strelSize);
Ie = imerode(img, se);
Iobr = imreconstruct(Ie, img);
Iobrd = imdilate(Iobr, se);
out = imreconstruct(imcomplement(Iobrd), imcomplement(Iobr));
out = imcomplement(out);
end</pre>
```

A.1.3 Marker controlled watershed function

```
function out = mwss(img)
img = morphRecon(img);
bw = ~im2bw(img(:,:,2),graythresh(img(:,:,2)));
```

```
%%
  D = -bwdist(~bw,'chessboard');
  mask = imextendedmin(D,2);
  D2 = imimposemin(D,mask);
  Ld2 = watershed(D2);
  out = bw;
  out(Ld2 == 0) = 0;
end
A.1.4 Concave points segmentation function
function stats = mia_particles_segmentation(I,param)
% mia_particles_segmentation performs segmentation by using the concave points.
% Synopsis
%
      stats = mia_segmentation_concave(I,k,thd1,thd2,thdn)
   Description
%
       Returns segmentation result (objects boundaries) of overlapping nanoparticles
%
       by using concave points and ellipse fitting propeties.
%
   Inputs
%
       - I
               grayscale or binary Image
       - k
%
               kth adjucnet points to the corner point
```

bw = imfill(bw,'holes');

- thd1

%

Euclidean distance between ellipse centroid of the

```
%
               combined contour segments and ellipse fitted to each segment
%
       - thd2
                 Euclidean distance between between the centroids of ellipse
               fitted to each segment.
%
%
       - thdn
                 Euclidean distance between contour center points
%
                to define neighbouring segments
                 visualize the contoure evidence extraction step
%
       - vis1
                 visualize the contoure estimation step
      - vis2
%
%
   Outputs
                cell array contating the objects boundaries
%
       - stats
%
   Authors
%
        Sahar Zafari <sahar.zafari(at)lut(dot)fi>
%
   Changes
%
%
      14/01/2016 First Edition
  % load the parameters
  k = param(1);
  thd1 = param(2);
  thd2 = param(3);
```

```
thdn = param(4);
  vis1 = param(5);
  vis2 = param(6);
  % Image Binarization by otsu's method
%
    I = morphRecon(I);
%
    level = graythresh(I);
    imgbw = \sim im2bw(I,level);
%
  imgbw = mwss(I);
  imgbw = fillBorderObjects(imgbw);
  % Contour Evidence Extraction
%
    fprintf('Performs Contour Evidence Extraction....\n')
  contourevidence = mia_cmpcontourevidence(imgbw,k,thd1,thd2,thdn,vis1);
  % Contour Estimation
%
    fprintf('Performs Contour Estimation....\n')
  stats = mia_estimatecontour_lsf(I,contourevidence,vis2);
end
function out_bw = fillBorderObjects(in_bw)
  bw_a = padarray(in_bw,[1\ 1],1,pre');
  bw a filled = imfill(bw a,'holes');
  bw_a_filled = bw_a_filled(2:end,2:end);
  bw_b = padarray(padarray(in_bw,[1 0],1,'pre'),[0 1],1,'post');
```

```
bw_b_filled = imfill(bw_b,'holes');

bw_b_filled = bw_b_filled(2:end,1:end-1);

bw_c = padarray(in_bw,[1 1],1,'post');

bw_c_filled = imfill(bw_c,'holes');

bw_c_filled = bw_c_filled(1:end-1,1:end-1);

bw_d = padarray(padarray(in_bw,[1 0],1,'post'),[0 1],1,'pre');

bw_d_filled = imfill(bw_d,'holes');

bw_d_filled = bw_d_filled(1:end-1,2:end);

out_bw = bw_a_filled | bw_b_filled | bw_c_filled | bw_d_filled;

end
```

Appendix B

B.1 Table of Equation

Sensitivity	$Sensitivity = \frac{TP}{TP + FN}$
Specificity	$Specificity = \frac{TN}{TN + FP}$
Positive predictive value	$PPV = \frac{TP}{TP + FP}$
Negative predictive value	$NPV = \frac{TN}{TN + FN}$
ANFIS node function	$Q_i^1 = \mu A_i(X)$
Gaussian membership function	$\mu A_i(X) = exp\left\{-\frac{1}{2}\frac{(X-C_i)^2}{\sigma_i^2}\right\}$
Node interconnecting signal multiplication	$w_i = \mu A_i(X_1) \times \mu B_i(X_2), i = 1,2$
of the i-th rule's firing strength	$w_i^- = \frac{w_i}{w_1 + w_2}$
adaptive node	$Q_i^4 = w_i^- f_i = w_i^- (m_i X_1 + n_i X_2 + q_i), i = 1,2$
weighted average of all incoming signals	$Q_i^5 = \sum_i w_i^- f_i = \frac{\sum_i w_i f_i}{\sum_i w_i}, i = 1,2$

the overall output (f) of the learning process	$f = \frac{w_1}{w_1 + w_2} f_1 + \frac{w_2}{w_1 + w_2} f_2 = w_1^- f_1 + w_2^- f_2$ $= (w_1^- X_1) m_1 + (w_1^- X_2) n_1 + (w_1^-) q_1 + (w_2^- X_2) m_2$ $+ (w_2^- X_2) n_2 + (w_2^-) q_2$
variance	$\sigma_b^2 = \omega_0(t)\omega_1(t)[\mu_0(t) - \mu_1(t)]^2$
Chebyshev distance	$D_{chess} = \max(x_2 - x_1 , y_2 - y_1)$
segment grouping	$ADD_{S_i \cup S_j} \le ADD_{S_i},$ $ADD_{S_i \cup S_j} \le ADD_{S_j}$
Fitting ellipse of segment group	$ADD_{S_i} = \frac{1}{n} \sum_{k=1}^{n} \sqrt{(x_k - x_{f,k})^2 + (y_k - y_{f,k})^2}$
fitting ellipse transform coordinates	$\begin{bmatrix} x'_k \\ y'_k \end{bmatrix} = \begin{bmatrix} \cos \emptyset & -\sin \emptyset \\ \sin \emptyset & \cos \emptyset \end{bmatrix} \begin{bmatrix} x_k & -x_{eo} \\ y_k & -y_{eo} \end{bmatrix}$
Simplified version of ADD _{si}	$ADD_{S_i} = \frac{1}{n} \left[\sum_{k=1}^{n} \sqrt{{x'}_k^2 + {y'}_k^2 (1 - \frac{1}{ D_k })} \right]$
D_k	$D_k^2 = \frac{{x'}_k^2}{a^2} + \frac{{y'}_k^2}{b^2}$
ADD with contour longer than segment it self	$ADD_{S_i \cup S_j} \le \omega_i ADD_{S_i},$ $ADD_{S_i \cup S_j} \le ADD_{S_j}$
Wi	$\omega_i = \frac{l_i}{l_i + l_j}$

Distance				
between Ellipse	$d(e_i,e_{ij}) > t_1$			
centroid and the first	$dig(e_i,e_{ij}ig)>\ t_1$ $dig(e_j,e_{ij}ig)>\ t_1$			
threshold				
Distance				
between Ellipse	1()>+			
centroid and the	$d(e_i, e_j) > t_2$			
second threshold				
Area of cell	$Area(R) = Total\ Number\ of\ pixels(R)$			
compactness	$compactness(R) = \frac{2\sqrt{\pi Area(R)}}{perimeter(R)}$			
Form factor	$form \ factor(R) = \frac{4\pi Area(R)}{perimeter^2}$			
GLCM co- occurrence matrix	$C_{\Delta x, \Delta y}(i, j) = \sum_{x=1}^{n} \sum_{y=1}^{m} \begin{cases} 1 & \text{if } I(x, y) = i \ I(x + \Delta x, y + \Delta y) = j \\ 0 & \text{Otherwise} \end{cases}$			
Dissimilarity	$rac{1}{2}\sum_{i=1}^N\left rac{b_i}{B}-rac{w_i}{W} ight $			
Inverse difference moment	$IDM = \sum_{i=0}^{G-1} \sum_{j=0}^{G-1} \frac{1}{1 + (i-j)^2} P(i,j)$			
Mean	$M1(k,l) = \frac{1}{NR} \sum_{mn \in R} \sum [u(m-k, n-l)]$			
Skewness	$M5(k,l) = \frac{1}{NR} \sum_{mn \in R} \sum [u(m-k, n-l) - Ml(k,l)]_{3}$			

kurtosis	$M6(k,l) = \frac{1}{NR} \sum_{mn \in R} \sum_{mn \in R} [u(m-k,n-l) - M1(k,l)]_{4}$
Standard deviation	$M3(k,l) = \sqrt{\frac{1}{NR} \sum_{mn \in R} \sum_{l} [u(m-k,n-l) - M1(k,l)]}_{2}$